MASTER COPY

OAK RIDGE NATIONAL LABORATORY

operated by

UNION CARBIDE CORPORATION

for the

U.S. ATOMIC ENERGY COMMISSION

ORNL-TM-122

UNIT OPERATIONS SECTION MONTHLY PROGRESS REPORT

NOVEMBER 1961

NOTICE

This document contains information of a preliminary nature and was prepared primarily for internal use at the Oak Ridge National Laboratory. It is subject to revision or correction and therefore does not represent a final report. The information is not to be abstracted, reprinted or otherwise given public dissemination without the approval of the ORNL patent branch, Legal and Information Control Department.

LEGAL NOTICE

This report was prepared as an account of Government sponsored work. Neither the United States, nor the Commission, nor any person acting on behalf of the Commission:

A. Makes any warranty or representation, expressed or implied, with respect to the accuracy, completeness, or usefulness of the information contained in this report, or that the use of any information, apparatus, method, or process disclosed in this report may not infringe privately owned rights; or

B. Assumes any liabilities with respect to the use of, or far damages resulting from the use of any information, apparatus, method, or process disclosed in this report.

As used in the above, "person acting on behalf of the Commission" includes any employee or contractor of the Commission, or employee of such contractar, to the extent that such employee or contractor of the Commission, or employee of such contractor prepares, disseminates, or provides access to, any informatian pursuant to his employment or contract with the Commission, or his employment with such contractor.

ORNL-TM-122

UNIT OPERATIONS SECTION MONTHLY PROGRESS REPORT

November 1961

CHEMICAL TECHNOLOGY DIVISION

M. E. Whatley

P. A. Haas
R. W. Horton
A. D. Ryon
J. C. Suddath
C. D. Watson

Date Issued

MAY 16 1962

OAK RIDGE NATIONAL LABORATORY
Oak Ridge, Tennessee
Operated By
UNION CARBIDE CORPORATION
for the
U. S. Atomic Energy Commission

ABSTRACT

Operation of a 6-in.-dia foam separation column with Sr-89 tracer and dodecylbenzenesulfonate as a surfactant and foaming agent was continued. The catalytic oxidation of H_2, CO, and CH_4 was studied using a nickel-chrome-palladium ribbon catalyst. A Mark I prototype fuel assembly was sheared to within 1-1/2-in. of the end by modifying the gag hydraulic system of the shear. The force required to shear a highly carburized Mark I fuel assembly (1.7-2.7% C) was ~25 tons compared to ~50 tons for the ductile tubing. Demonstration of the mechanical dejacketing of the SRE Core I fuel burned to ~675 mwd/ton and cooled about 2 years is complete, and decontamination and equipment removal from the segmenting cell is approximately 90% completed. Ten SRE Core I fuel jackets were dissolved in aqua regia and analysis showed negligible uranium and Pu. A semicontinuous leach run, in which -2 mesh graphite fuel containing 2.6% uranium was leached in 90% HNO_3 at 60°C, gave only 0.37% uranium loss. Graphically estimated spectral factors for radiation between tubes within fuel bundles and improved wall radiation factors were used to calculate the temperature distribution expected within spent fuel elements. Further studies of the dissolution of zirconium oxide by HF in fused salt resulted in rates about twice as great as for Zr metal under similar conditions.

CONTENTS

		Page
	Abstract	2
	Previous Reports in this Series for the Year 1961	4
	Summary	5
1.0	Chemical Engineering Research	7
2.0	GCR Coolant Purification Studies	12
3.0	Power Reactor Fuel Processing	31
4.0	Reactor Evaluation Studies	43
5.0	Volatility	49

Previous Reports in this Series for the Year 1961

January	ORNL CF 61-1-27
February	ORNL CF 61-2-65
March	ORNL CF 61-3-67
April	ORNL-TM-32
May	ORNL-TM-33
June	ORNL-TM-34
July	ORNL-TM-35
August	ORNL-TM-65
September	ORNL-TM-112
October	ORNL-TM-121

All previous reports in this series are listed in the June 1961 report, ORNL-TM-34, from the beginning December 1954.

SUMMARY

1.0 CHEMICAL ENGINEERING RESEARCH

Operation of a 6-in.-dia foam separation column with Sr-89 tracer and dodecylbenzenesulfonate as a surfactant and foaming agent was continued. The surfactant distributions for two batch runs were $\Gamma/c = 5.6$ to 5.9×10^{-4} (moles/cm^2)(moles/cm^3) for concentrations below 250 ppm and $\Gamma = 3.2 \times 10^{-10}$ moles/cm^2 for 500 ppm. Values for Γ/c for Sr were 1.1 to 3.6×10^{-3} (moles/cm^2)(moles/cm^3), but the Sr-89 material balances were about 60%. An air operated whistle or "Sonic Airjet Defoamer" was tested and installed in place of the cyclone defoamer and it is more convenient for the 6-in.-dia column foam breaker.

2.0 GCR COOLANT PURIFICATION STUDIES

The catalytic oxidation of H_2, CO and CH_4 was studied using a nickel-chrome-palladium ribbon catalyst. Mass transfer of the contaminant and oxygen to the reaction site from the bulk gas contributed to the reaction rate control. The reaction rate constants for the three contaminants was fitted to an Arrhenius-type expression.

3.0 POWER REACTOR FUEL PROCESSING

3.1 Shear and Leach

Spring loading the inner gag hydraulic cylinder and reducing the hydraulic pressure to zero at the time the fuel bundle is being moved forward resulted in a porcelain filled Mark I prototype fuel assembly being sheared to within 1-1/2 in. of the end.

Shearing into the flat side of a fuel assembly with the stepped blade resulted in producing discrete pieces; however, the tubes were badly spread causing drag back when the movable blade was retracted.

The force required to shear a highly carburized Mark I fuel assembly (1.7-2.7% C) was ~25 tons as compared to ~50 tons for the ductile tubing.

A 2.25 liter bulk volume is the optimum solids batch size for the leacher to insure the solids being covered with the acid dissolvent.

3.2 SRE Dejacketing Studies

Demonstration of the mechanical dejacketing of the SRE Core I fuel burned to ~675 mwd/ton and cooled about 2 years is complete, and decontamination and equipment removal from the segmenting cell is approximately 90% completed.

Batch dissolution of ten SRE Core I fuel jackets, 304-L stainless steel, 10 mil wall, was successfully completed in aqua regia of 2 M HCl-5 M HNO_3 and 3 M HCl and 4 M HNO_3 concentrations. Using an initial molar ratio of Cl^- to stainless steel of 3.5 to 1 the stainless steel jackets were

completely dissolved in 3 out of 5 batch dissolutions, yielding solutions containing 50 g of stainless steel per liter. The 2 M HCl-5 M HNO_3 solution where the Cl^- to stainless steel ratio was 2.35 to 1 did not completely dissolve the jackets and a cleanup run was always required. Analysis of the product solutions show a negligible uranium loss from the dejacketing operation. Low concentrations of U from 0.001 to 0.0041 mg/ml or from 0.1 to 4.6 mg U/mole stainless steel, and Pu from 108 to 1.1×10^3 c/m/ml were measured. A spectrophotometric scan of the dissolved jacket showed a complete absence of fission products originating from the core fuel.

3.3 U-C Fuel Processing

A uranium loss of only 0.37% (100 ppm U in residue) was sustained in a semicontinuous leach run in which -2 mesh (73% > 12 mesh) graphite fuel containing 2.6% uranium was leached in 90% HNO_3 at 60°C, a 2 hr batch leach, a 4 hr leach in flowing acid, and a final water wash. Uranium loss for -4 mesh (27% > 12 mesh) fuel following identical treatment was 1.6%.

4.0 REACTOR EVALUATION STUDIES

Graphically estimated spectral factors for radiation between tubes within fuel bundles and improved wall radiation factors were used to calculate the temperature distribution expected within spent fuel elements if all heat transfer were by radiation. These results are believed to give a much more realistic picture of the effects of radiation within air filled casks than previous calculations. Although the previous results gave better agreement with the experimental data which are available on center tube temperatures, the more recent calculations give a better fit to the temperature distribution throughout the bundle. The calculated results are always slightly higher than the experimental since convection and conduction were neglected.

5.0 VOLATILITY

Further studies of the dissolution of zirconium oxide by HF in fused salt resulted in rates about twice as great as for Zr metal under similar conditions. Preliminary chemical analyses of the film forned on partially dissolved oxide indicate that an intermediate oxyfluoride may be formed.

1.0 CHEMICAL ENGINEERING RESEARCH

1.1 Foam Separation - P. A. Haas, J. D. Sheppard

Continuous countercurrent and batch operation of a 6-in.-ID foam-liquid column was continued to study engineering variables controlling column performance. Mechanical operation of the column system was improved. Complete material balances for the Sr-89 tracer and satisfactory isotopic exchange for Sr during countercurrent column operation were not demonstrated.

Batch Run Results. Results are complete for two batch tests (runs 11 and 12) made with initial charges of seven liters of 10^{-3} M NaOH with $Sr(OH)_2$ and Trepolate F-95 to give Sr/dodecylbenzenesulfonate mole ratios of 0.2. The N_2 used to generate the foam was bubbled through 0.2 M NaOH prior to metering at 3,000 cc/min into the column. Liquid and condensed foam samples were taken (Figures 1.1 and 1.2) at 5 min intervals. The condensed foam sample times were corrected for the column holdup which was about 5 min of normal gas flow or 7 min from the start of foaming until collection of condensed foam.

Calculated surfactant material balances were 91% for run 11 and 102% for run 12. The β material balances were 62% for run 11 and 60% for run 12.

Values for Γ or Γ/c for the dodecylbenzenesulfonate may be calculated from the surfactant analyses (Figure 1.1). For run 11 at zero time, the surfactant rate in excess of that corresponding to the liquid volume of the condensed foam is:

$$\left(47\ \frac{\mu\ \text{moles}}{\text{min}}\right) - \left(0.012\ \frac{\ell}{\text{min}}\right)\left(250\ \frac{\mu\ \text{mole}}{\ell}\right) = 44\ \frac{\mu\ \text{mole}}{\text{min}}$$

For a surface area of 100 cm^2/cm^3 for the foam as generated:

$$\frac{\Gamma}{c} = \frac{44 \times 10^{-6}}{100 \times 300}\ \frac{1000}{250 \times 10^{-6}} = 5.9 \times 10^{-4}\ \text{cm}$$

Similarly at 20 min, $\Gamma/c = 5.6 \times 10^{-4}$ cm. The surfactant concentrations for run 12 are greater than the critical micelle concentration reported in laboratory studies. Therefore, the surface excess would be controlled by the saturation of surface leaving the column and Γ could be calculated as

$$\left(\frac{98\ \mu\ \text{moles}}{\text{min}}\right) - (0.040)(1250) = 48\ \frac{\mu\ \text{moles}}{\text{min}}$$

$$\frac{48 \times 10^{-6}}{50 \times 3000} = 3.2 \times 10^{-10}\ \text{moles/cm}^2$$

The collapse of bubbles throughout the column results in a change in surface area from 100 cm^2/cm^3 foam near the foam-liquid interface to as low as 50 cm^2/cm^3 foam or less for the foam leaving the column. For low liquid surfactant concentrations, the surface in equilibrium with the liquid

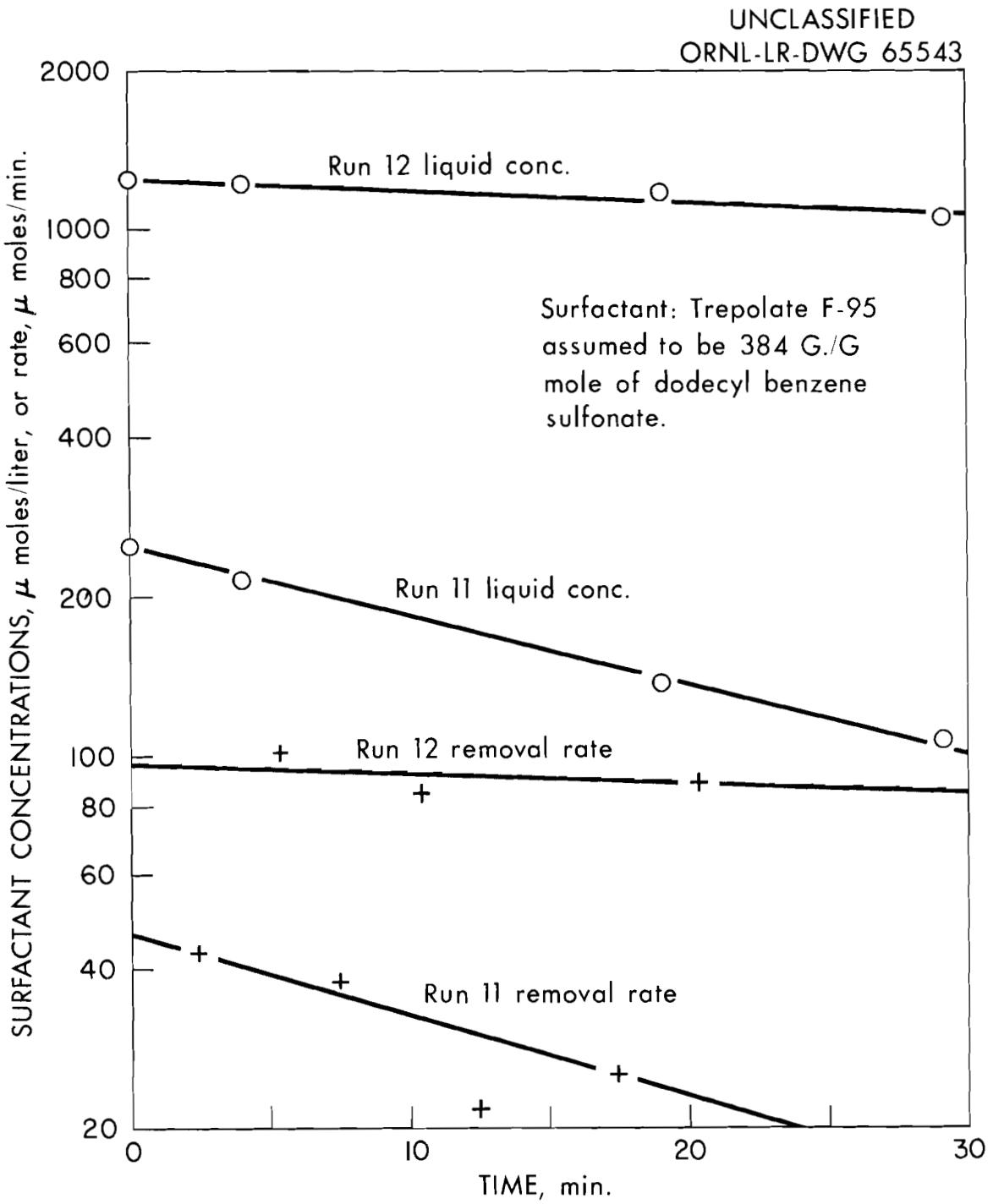

Fig. 1.1. Surfactant analyses – Runs 11 and 12.

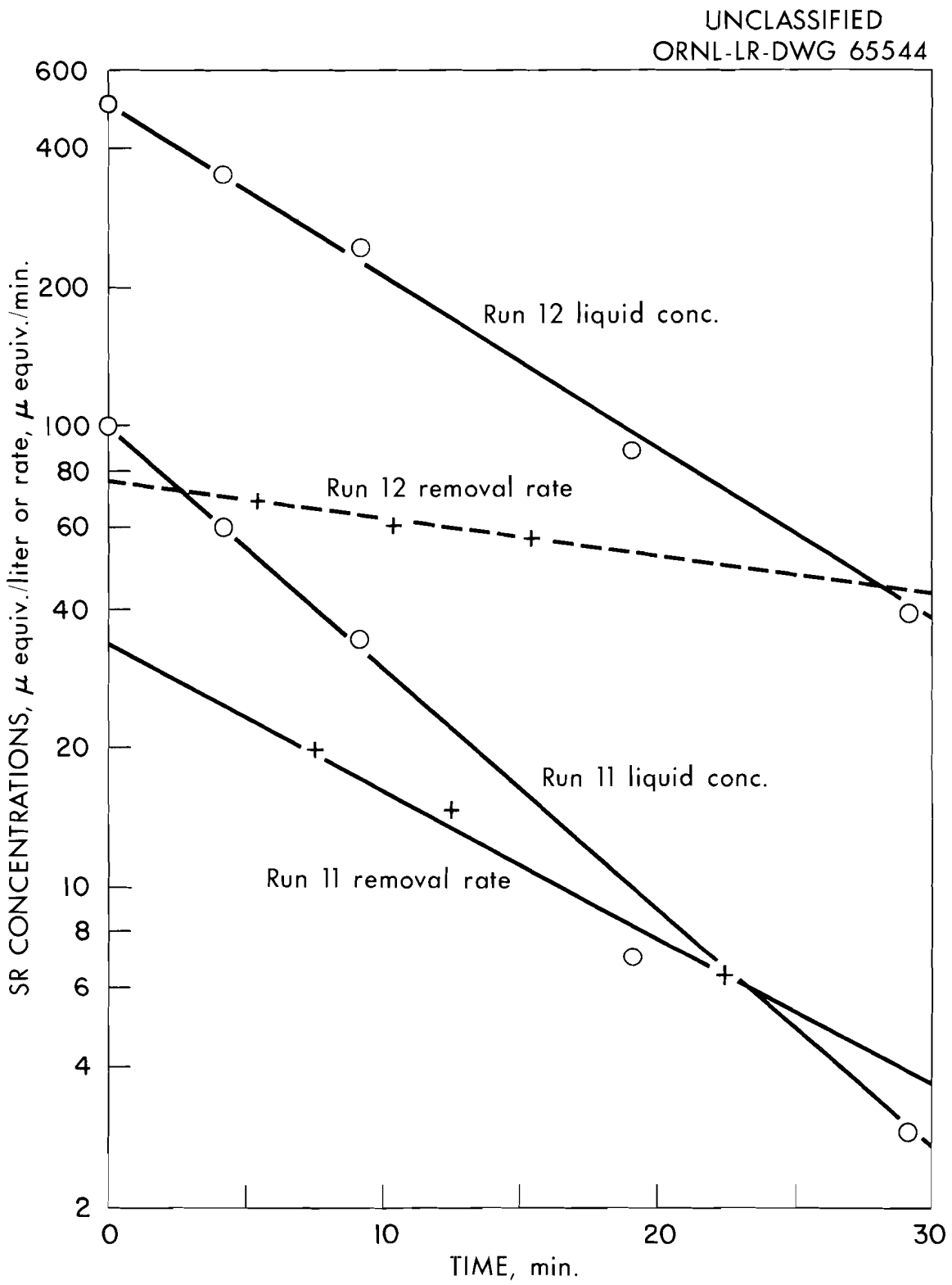

Fig. 1.2. SR from gross β analyses – Runs 11 and 12.

is only partly covered with surfactant. Then a disappearance of surface only results in an increased saturation of the remaining surface. For surfactant concentrations in the liquid above the critical micelle concentration, the surface has a constant concentration and disappearance of surface results in recycle of surfactant to the liquid. Based on these effects, the surface areas used for calculations for the surfactant were 100 cm^2/cm^3 for Γ/c for run 11 and 50 cm^2/cm^3 for Γ for run 12.

Values of Γ/c for Sr may be calculated from the β analyses shown in Figure 1.2 if it is assumed that there is no reflux of Sr (Table 1.1).

Table 1.1. Calculated Values of Γ/c for Sr-run 11

Time min	Sr Conc. in Liquid $\frac{\mu \text{ equiv}}{\text{liter}}$	Sr Rate in Cond. Foam $\frac{\mu \text{ equiv}}{\text{min}}$	Excess Sr in Foam $\frac{\mu \text{ equiv}}{\text{min}}$	Γ/c[a] 10^{-3} $\frac{\text{moles/cm}^2}{\text{moles cm}^3}$ or 10^{-3} cm
0	100	33.5	32	1.1
5	55	23.3	22.5	1.4
10	30	16.0	15.7	1.7
15	16.4	11.2	11.0	2.2
20	9.0	7.7	7.6	2.8
25	4.9	5.3	5.3	3.6
20[b]	90	53.0	49.0	1.8

[a]For an area of 3×10^5 cm^2/min

[b]For run 12

Sonic Foam Breaker. A TEKNIKA Sonic Airjet Defoamer was tested, installed, and used as a foam breaker for runs 11, 12, and 13. This unit is rated to produce high intensity directional sound at 12,000 cycles/sec when supplied with 15 SCF of air at 30-40 psi. When tested in the 6-in.-ID column about 24-in. above the liquid-foam interface, it easily kept the foam 6 in. or more below the defoamer for foam rates up to 4000 cc/min (the maximum tested). The unit was installed within a foam breaker chamber vented to the cell off-gas. It easily breaks high rates of wet foam, but the dry foam which results at low rates is sometimes difficult to break. Distilled water or dilute HCl introduced through a capillary feed line installed below the defoamer helps foam condensation for dry foam and dilutes the condensed foam to avoid precipitation of solids. When the sonic defoamer was operated with 10 cc/min of liquid and no foam, liquid collected at a 6.2 cc/min rate indicating 3.8 cc/min of evaporation.

In comparison with the previously used cyclone foam breaker, the sonic defoamer is more convenient for the present relatively small system. The vacuum used to operate the cyclone required both a pump for condensed foam removal and a "hot" vacuum pump because of the Sr-89 tracer. Condensation of more complete for the sonic defoamer. The 0.4-in.-dia cyclone appears to have a much larger capacity (> 20 liter/min), does not generate the large volume of off-gas, and would probably be preferred for larger columns.

Column Alterations. Gold-platinum alloy spinerettes like those used by the rayon industry had generated very uniform bubbles in small scale foam separation studies. A 2-in.-dia spinerette with approximately 1800 50μ dia holes was installed and tried in the 6-in.-dia column. Three extra coarse fritted glass gas dispersion tubes were also installed and tried in the same column end plate. These gave much finer and less uniform bubbles than the spinerettes. Use of these two types of dispersors separately and together will permit study of bubble size and size distribution as a parameter.

2.0 GCR COOLANT PURIFICATION STUDIES

J. C. Suddath

Contamination of coolant gases by chemical impurities and release of fission products from fuel elements are major problems in gas-cooled reactors and in-pile experimental loops. Investigations are being made to determine the best methods to reduce the impurities, both radioactive and non-radioactive, with emphasis on the kinetics of the oxidation of hydrogen, carbon monoxide, and methane by oxygen in the proposed EGCR catalytic oxidizer.

The catalyst to be used in the EGCR helium purification system is Ni-Cr metal ribbon with activated Pd on its surface. This catalyst is manufactured by the American Metals Products Co. A short experimental investigation of the effectiveness of this catalyst for the oxidation of H_2, CO, and CH_4 by O_2 was made over the range of anticipated operating conditions expected in the EGCR. Correlations of the effects of the various parameters have been made. It was found that the present design of the EGCR catalytic oxidizer is inadequate over a portion of the stated proposed operating conditions unless oxygen contamination in the coolant is accepted.

2.1 Specifications and Properties of EGCR Catalytic Oxidizer - C. D. Scott

The catalytic oxidizer furnished by American Metals Products Co. is a vessel 8-in.-ID by 7.5-in.-deep filled with their nickel-chromium-palladium ribbon catalyst.

Properties of Catalyst. The catalyst is in the form of nickel-chromium metal ribbon coated with activated palladium. A typical chemical composition of the three components in the catalyst is:

Nickel - 58.3%
Chromium - 31.3%
Palladium - 1.1%

The ribbon is metallic in form and has the following dimensions:

Length - variable
Width - 0.036-0.037 inches
Depth - 0.005-0.006 inches

The packed density of the ribbon catalyst in a small catalytic unit obtained from the company was 0.384 g/cc. Specific surface area was approximately equal to the exterior surface of the ribbon.

Catalytic Unit Specifications.[1-3] The design specifications for the EGCR catalytic unit are as follows:

Inlet gas (300 psia and 260°C to 700°C)

Component	Vol %
He	95.0
CO	2.3 max
H_2	2.3 max
CO_2	0.2
N_2	0.1
H_2O	trace
Hydrocarbons	trace
Fission products	trace

Effluent gas (based on 650°C inlet and 300 psia)

Component	Maximum Content ppm by vol
CO	1000
H_2	1000

Gas feed rate to oxidizer:

130 lb/hr or 0.82 g-moles/cm^2-min

2.2 Experimental Work

Reagents. The gases used in the tests were of the following grades:

Helium	Navy Grade A, purity ~100%
Hydrogen	99.5% purity
Carbon Monoxide	99.5% purity
Methane	99.0% purity
Oxygen	99.5% purity

Experimental Facility. All tests were made in the Gas-Cooled Reactor Helium Coolant Purification Test Facility[4] (Figure 2.1). This facility is capable of synthesizing contaminated helium with hydrogen, carbon monoxide, and methane, and oxygen addition to the contaminated gas is possible.

The 2-in.-dia oxidizers which are components of the system were used in this study. Oxidizers were fabricated from 2-in.-dia schedule 80 stainless steel pipe with high-pressure (600 psi) flanges at either end (Figure 2.2). Catalyst bed depths of 1 to 4 in. were used in the oxidizers with thermocouple probes every 2 in. within the vessels. Each oxidizer was internally insulated at the top and bottom and externally heated and insulated by a tube furnace. In some tests a 1-in.-ID insert was used in the oxidizer to allow higher gas mass velocities. Helium contaminated with 0-2% hydrogen, 0-2% carbon monoxide, 0-1% methane, and 0-2% oxygen at 0-325 psig, 30-600°C, and gas flow rates of 0-120 slpm can be delivered to the oxidizer.

UNCLASSIFIED
ORNL-LR-DWG 45353

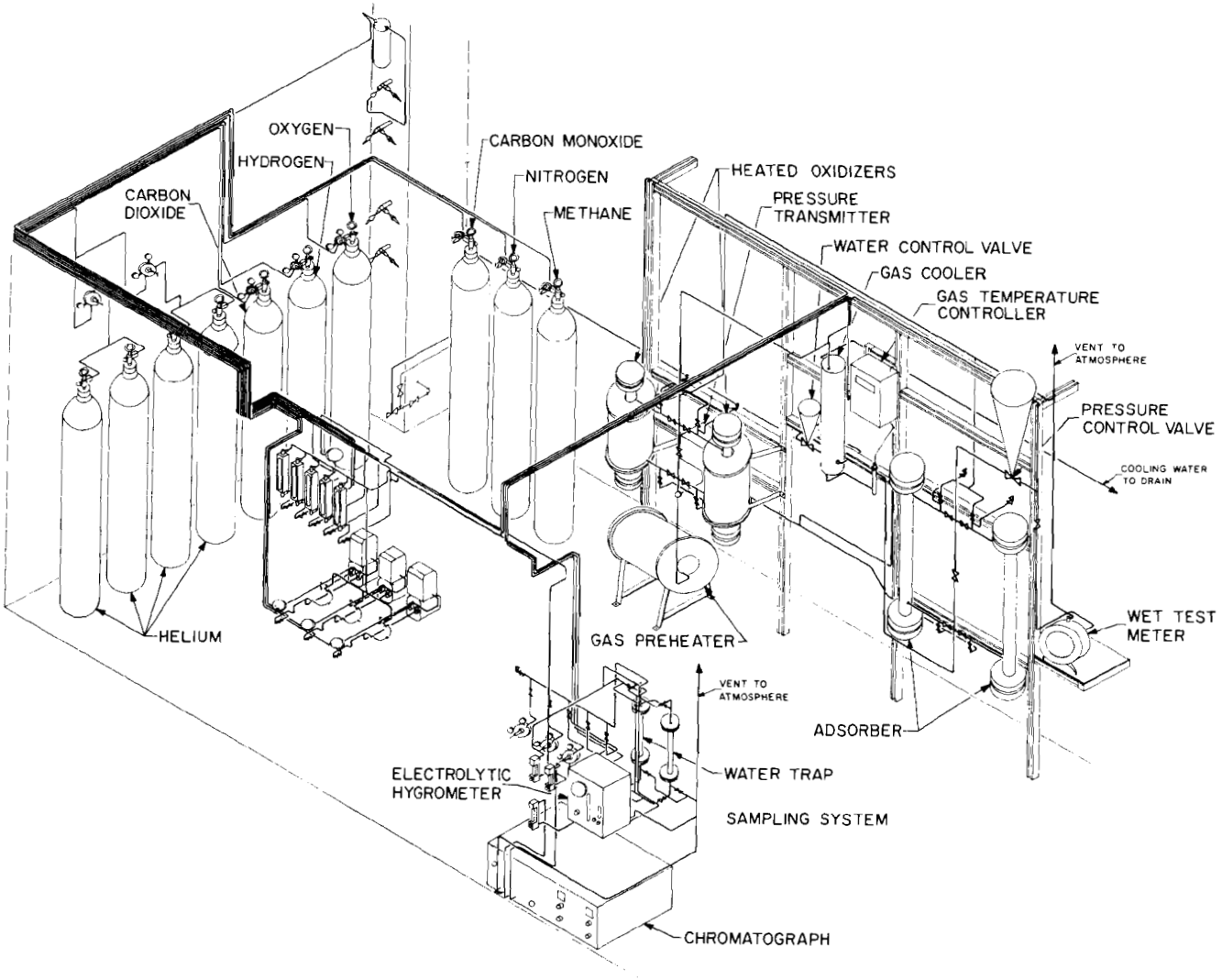

Fig. 2.1. GCR helium coolant purification test facility.

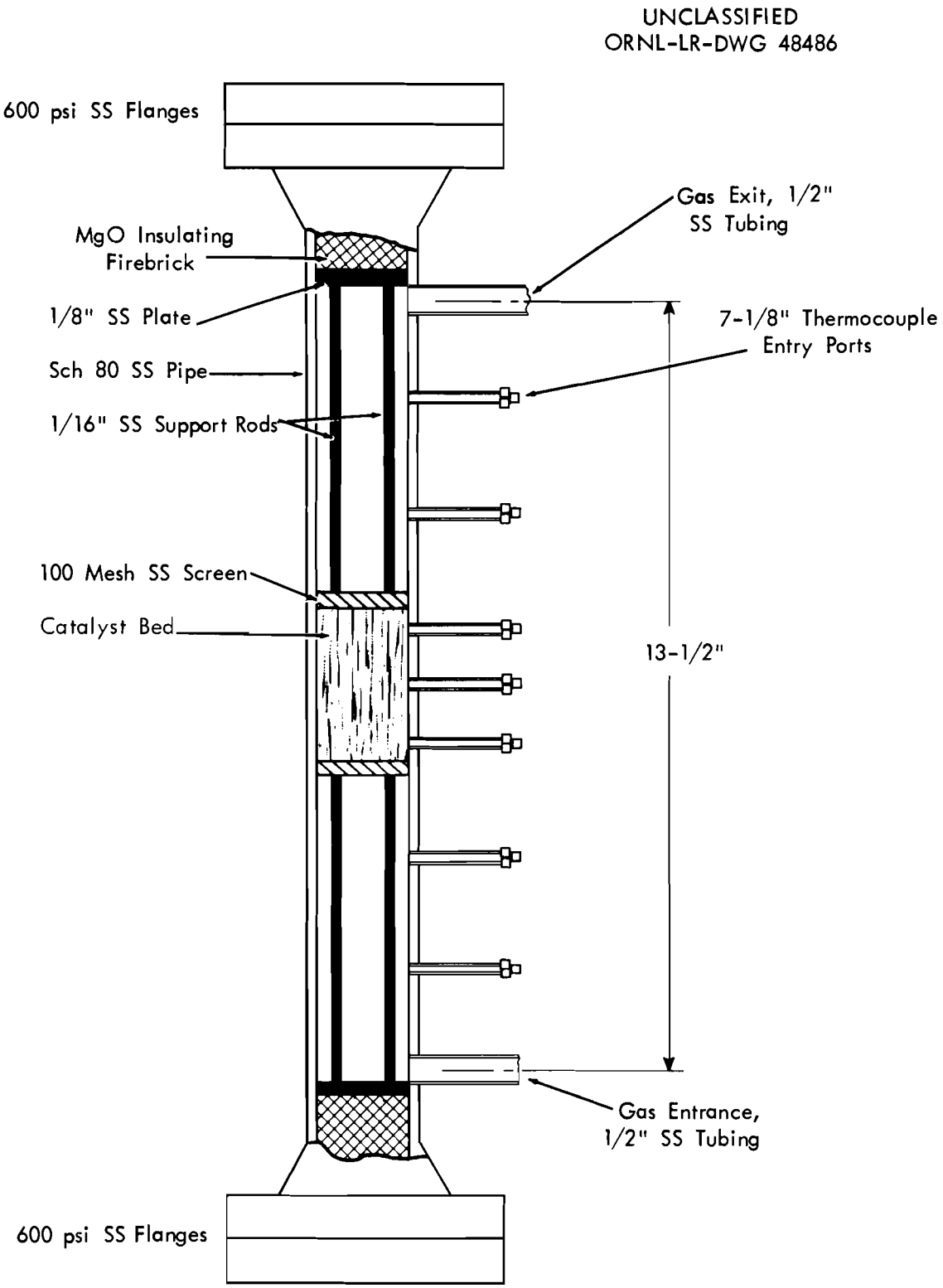

Fig. 2.2. 2-in. oxidizer in helium purification test facility without external heater.

Experimental Procedure. All tests were made by the following procedure:

1. The oxidizer was charged with the proper amount of catalyst and heated to the specified operating temperature.

2. A preheated stream of pure helium was then introduced to the oxidizer and the catalyst bed was allowed to reach thermal equilibrium.

3. A predetermined, constant rate of contaminant (hydrogen, carbon monoxide, or methane) was introduced to the gas stream.

4. Oxygen was introduced to the gas mixture just prior to its entry to the 2-in. oxidizer or to a point just below the catalyst bed at an initial, constant rate less than that required to give a stoichiometric amount.

5. The oxygen flow rate was increased as a step function periodically until there was no contaminant (H_2, CO, or CH_4) in the reactor off-gas or until the oxygen addition rate was greater than necessary to give a stoichiometric amount.

6. The oxidizer off-gas was sampled periodically by a gas adsorption chromatograph using comparative thermal conductivity measurements, and check samples were taken for analysis by mass spectrometry. The lower limit of detection of hydrogen by the chromatograph was ~10 ppm and for the oxygen, carbon monoxide, and methane was ~5 ppm.

Experimental Data. From the experimental data taken, it was possible to determine the oxygen and contaminant concentration in the helium gas stream prior to its entry to the oxidizer and in the oxidizer off-gas. Thus, it was possible to determine the effectiveness of a specific amount of catalyst under the various experimental conditions.

Catalytic Oxidation of Hydrogen. Fourteen tests (Table 2.1a) were made at 400-600°C and 300 psia with catalyst bed depths of 1 to 4 in. in a 1-in.-ID and 2-in.-ID vessel for the catalyzed reaction, $H_2 + 1/2\ O_2 = H_2O$. Gas mass flow rates of 0.083 to 1.0 g mole/cm^2-min were used; and initial hydrogen concentrations were 0.51 to 1.96 vol %.

Catalytic Oxidation of Carbon Monoxide. Twelve tests (Table 2.1b) were made at bed temperatures of 400-600°C and a total pressure of 300 psia for the catalyzed reaction, $CO + 1/2\ O_2 = CO_2$. Gas mass flow rates of 0.083 to 1.0 g mole/cm^2-min were used and initial carbon monoxide concentration ranged from 0.44 to 2.47 vol %.

Catalytic Oxidation of Methane. Eight tests (Table 2.1c) were made at bed temperatures of 400-600°C and a pressure of 300 psia for the catalyzed reaction, $CH_4 + 2\ O_2 = CO_2 + 2\ H_2O$. Gas mass flow rates of 0.083 to 1.0 g mole/cm^2-min were used and the initial methane concentration ranged from 0.11 to 0.67 vol %.

Table 2.1. Experimental Data from the Kinetic Study of the Oxidation of Hydrogen, Carbon Monoxide, and Methane by Oxygen in a Fixed Bed of American Metals Products Ni-Cr-Pd Ribbon Catalyst

Run No.	Bed Temp., °C ± 10°C	Bed Dia, cm	Bed Vol, cc	Total Gas Flow Rate, g moles/min	Contaminant Concentration, mole fraction: Initial		Final	
a. Reaction $H_2 + 1/2\ O_2 = H_2O$					H_2	O_2*	H_2	O_2
1	500	5.0	100	3.28	0.010100	0.003807	0.002500	0.000007
2A	500	5.0	100	1.59	0.005100	0.002476	0.000200	0.000066
2B	500	5.0	100	1.59	0.005100	0.001860	0.001400	0.000010
3A	600	5.0	100	4.72	0.012500	0.004503	0.003500	0.000002
3B	600	5.0	100	4.72	0.012500	0.005572	0.001400	0.000022
4	600	5.0	100	3.28	0.019600	0.008911	0.001800	0.000011
5	500	5.0	100	3.28	0.018200	0.009146	0.000400	0.000246
6A	400	5.0	100	1.59	0.008000	0.003733	0.000600	0.000033
6B	400	5.0	100	1.59	0.008000	0.004243	0.000100	0.000293
7	600	5.0	100	3.28	0.010700	0.004552	0.001600	0.000002
8	500	5.0	100	4.72	0.012800	0.006380	0.000400	0.000180
9	500	2.5	56.6	4.72	0.014600	0.006642	0.001400	0.000042
10A	500	2.5	28.3	4.20	0.008100	0.003561	0.001600	0.000311
10B	500	2.5	28.3	4.20	0.008100	0.002469	0.003300	0.000169
11	400	2.5	28.3	4.20	0.007900	0.004810	0.000800	0.001260
12	500	2.5	28.3	4.20	0.017000	0.008007	0.001400	0.000207
13	400	2.5	28.3	4.20	0.011000	0.002801	0.005500	0.000051
14A	400	2.5	28.3	4.20	0.014300	0.004740	0.005500	0.000090
14B	400	2.5	28.3	4.20	0.014300	0.007260	0.001700	0.000960
14C	400	2.5	28.3	4.20	0.014300	0.007684	0.001000	0.001034
b. Reaction $CO + 1/2\ O_2 = CO_2$					CO	O_2*	CO	O_2
1A	500	5.0	100	3.28	0.010200	0.003657	0.002900	0.000007
1B	500	5.0	100	3.28	0.010200	0.004730	0.000700	0.000060
2	500	5.0	100	1.59	0.010000	0.004777	0.000500	0.000027
3	500	5.0	100	4.20	0.009600	0.004957	0.000300	0.000307
4	500	5.0	100	3.28	0.006700	0.002110	0.002500	0.000010
5	500	5.0	100	3.28	0.023000	0.010709	0.001600	0.000009
6A	400	5.0	100	3.28	0.012600	0.004706	0.003200	0.000006
6B	400	5.0	100	3.28	0.012600	0.005594	0.001500	0.000044

Table 2.1. (Continued)

Run No.	Bed Temp., °C ± 10°C	Bed Dia, cm	Bed Vol, cc	Total Gas Flow Rate, g moles/min	Contaminant Concentration, mole fraction			
					Initial		Final	
	b. Reaction $CO + 1/2\ O_2 = CO_2$				CO	O_2*	CO	O_2
7	600	5.0	100	3.28	0.012300	0.004902	0.002500	0.000002
8	500	2.5	56.6	4.20	0.004400	0.002280	0.000440	0.000300
9	400	2.5	28.3	1.59	0.011100	0.003327	0.004500	0.000027
10	400	2.5	28.3	1.59	0.024700	0.009693	0.005000	0.000043
11A	400	2.5	28.3	4.72	0.010700	0.002734	0.005000	0.000084
11B	400	2.5	28.3	4.72	0.010700	0.003734	0.003600	0.000184
11C	400	2.5	28.3	4.72	0.010700	0.005200	0.001700	0.000700
12	600	2.5	28.3	1.59	0.010100	0.005843	0.000020	0.000303
	c. $CH_4 + 2\ O_2 = CO_2 + 2\ H_2O$				CH_4	O_2*	CH_4	O_2
1	500	5.0	100	3.28	0.002900	0.001633	0.002600	0.001033
2	500	5.0	100	1.59	0.002600	0.003770	0.001520	0.001610
3	500	5.0	100	4.20	0.003400	0.002882	0.002600	0.001382
4	500	5.0	100	3.28	0.001100	0.000855	0.000970	0.000595
5	500	5.0	100	3.28	0.006700	0.002520	0.005800	0.000720
6	400	5.0	100	3.20	0.002300	0.001783	0.002100	0.001383
7	600	5.0	100	3.28	0.002100	0.001653	0.001600	0.000653
8	500	2.5	56.6	4.28	0.002000	0.002050	0.001900	0.001850

*Determined from stoichiometry.

Simultaneous Catalytic Oxidation of Hydrogen, Carbon Monoxide, and Methane. Three tests were made in which hydrogen, carbon monoxide, and methane were co-oxidized in two different catalyst bed sizes at 500°C (Table 2.2). In these tests a total pressure of 300 psia was used with mass flow rates of 0.171 and 0.220 g mole/cm^2-min. Initial contaminant concentrations varied from 0.44 to 1.40 vol %.

2.3 Correlation of Data

Since the purpose of this experimental study was to obtain experimental kinetic data and usable reactor design equations in a short time, no attempt was made to design the experimental program toward obtaining enough data with sufficient accuracy to permit determination of the mechanism of reaction rate control. This type of approach, as presented by Smith[5] and others, requires investigation of a considerable number of process variables and a large effort directed toward calculation and analysis of experimental results.

The approach taken was to empirically correlate the experimental data in a manner similar to that outlined by Waller[6] and used in an earlier report by the author.[7]

Apparent Reaction Rate. It was found that the apparent reaction rate for the oxidation of hydrogen, carbon monoxide, and methane at a constant mass flow rate and pressure could be expressed by

$$r = K\, y_c\, y_O \tag{1}$$

where

r = apparent reaction rate, g moles of contaminant reacted per cubic centimeter of catalyst bed per minute

K = apparent reaction rate constant at constant flow rates, g-moles/cc-min

y_c, y_O = mole fraction of contaminant and oxygen in the gas stream at any point in the reactor

The material balance around a differential volume in the reactor results in the flow reactor design equation[7]

$$\frac{V}{F} = -\int_{y_o}^{y_f} \frac{dy}{r} \tag{2}$$

where

V = volume of catalyst in reactor, cc

Table 2.2. Experimental Results of Simultaneous Catalytic Oxidation of Hydrogen, Carbon Monoxide, and Methane at 500 ± 12°C in a Flowing Stream of Helium

Run No.	Bed Dia, cm	Bed Volume, cc	Total Gas Flow Rate, g-moles/min	Initial Contaminant Concentration, mole fraction				Final Contaminant Concentration, mole fraction			
				H_2	CO	CH_4	O_2*	H_2	CO	CH_4	O_2
1A	5.0	100	3.28	0.014000	0.008300	0.011600	0.00975	0	0.0028	0.0116	0
1B	5.0	100	3.28	0.014000	0.008300	0.011600	0.01557	0	0	0.0098	0.00082
2A	5.0	100	3.28	0.004800	0.004400	0.011500	0.01272	0	0	0.0081	0.00132
2B	5.0	100	3.28	0.004800	0.004400	0.011500	0.00705	0.0004	0.0019	0.0096	0
3A	2.5	56.6	4.20	0.013600	0.007300	0.011700		0.0079	0.0063	0.0117	0
3B	2.5	56.6	4.20	0.013600	0.007300	0.011700		0.0010	0.0051	0.0117	0
3C	2.5	56.6	4.20	0.013600	0.007300	0.011700		0	0.0019	0.0112	0.00075

* Determined from stoichiometry.

F = gas feed rate, cc/min

y_o, y_f = mole fraction of contaminant initially and finally

Incorporation of eq. (1) individually into the flow reactor design equation with the correct stoichiometry, after integration, results in the following equations for determining the apparent reaction rate constant:

For hydrogen,

$$K_H = \frac{1}{(V/F)\left(y_{H_o} - 2y_{O_o}\right)} \ln \frac{y_{H_f}\, y_{O_o}}{y_{H_o}\, y_{O_f}} \tag{3}$$

For carbon monoxide,

$$K_C = \frac{1}{(V/F)\left(y_{C_o} - 2y_{O_o}\right)} \ln \frac{y_{H_f}\, y_{O_o}}{y_{C_o}\, y_{O_f}} \tag{4}$$

For methane,

$$K_{CH} = \frac{1}{(V/F)\left(2y_{CH_o} - y_{O_o}\right)} \ln \frac{y_{CH_f}\, y_{O_o}}{y_{CH_o}\, y_{O_f}} \tag{5}$$

where

y_{H_o}, y_{C_o}, y_{CH_o}, y_{O_o} = initial mole fraction of H_2, CO, CH_4, and O_2

y_{H_f}, y_{C_f}, y_{CH_f}, y_{O_f} = final mole fraction of H_2, CO, CH_4, and O_2

All three reaction rate constants were found to be temperature and mass-flow-rate dependent (Table 2.3).

The apparent reaction rate constant at constant mass flow rate can be incorporated into an expression for a rate constant for any flow rate which is dependent only on temperature:

$$K = kG^{\theta}, \qquad k = K/G^{\theta} \quad \text{or} \tag{6}$$

$$\log K = \log k + \theta \log G \tag{7}$$

where

k = rate constant for any mass flow rate dependent only on temperature

Table 2.3. Effect of Temperature and Mass Flow Rate on the Reaction Rate Constants

Contaminant	Temperature, °C	Average Reaction Rate Constant, K x 10^{-4} Mass flow rate, g-mole/cm²-min 0.083	0.17	0.24	0.33	0.88	1.00
H_2	400	14.3	-	-	-	22.7	-
H_2	500	21.3	22.2	34.3	-	40.4	70.1
H_2	600	-	35.2	42.8	-	-	-
CO	400	-	12.5	-	13.3	-	25.2
CO	500	22.2	24.5	28.1	-	39.4	-
CO	600	-	30.6	-	-	52.1	-
CH_4	400	-	0.59	-	-	-	-
CH_4	500	1.02	1.23	1.92	-	2.88	-
CH_4	600	-	2.98	-	-	-	-

G = mass flow rate, g moles/cm²-min

Θ = exponent of G necessary for correlation

A plot of log K vs log G should have an intercept of k and a slope of Θ for each component at each temperature. From these plots (Figures 2.3, 2.4, and 2.5) the following average values for Θ were determined.

$$\Theta_{H_2} = 0.37$$

$$\Theta_{CO} = 0.34$$

$$\Theta_{CH_4} = 0.51$$

The average values of the reaction rate constant k, determined at 400, 500, and 600°C for each contaminant from eq. (6) are plotted in an Arrhenius-type plot to obtain the temperature dependence of k (Figure 2.6). Assuming that k can be expressed with an Arrhenius-type expression,

$$\ln k = \ln A - E/RT \qquad (8)$$

Determination of the intercept and slope from these plots allow determination of the following expressions for the reaction rate constants, k,

For hydrogen,

$$k = 1.95 \times 10^{6} e^{-2200/RT} \qquad (9)$$

UNCLASSIFIED
ORNL-LR-DWG 64269

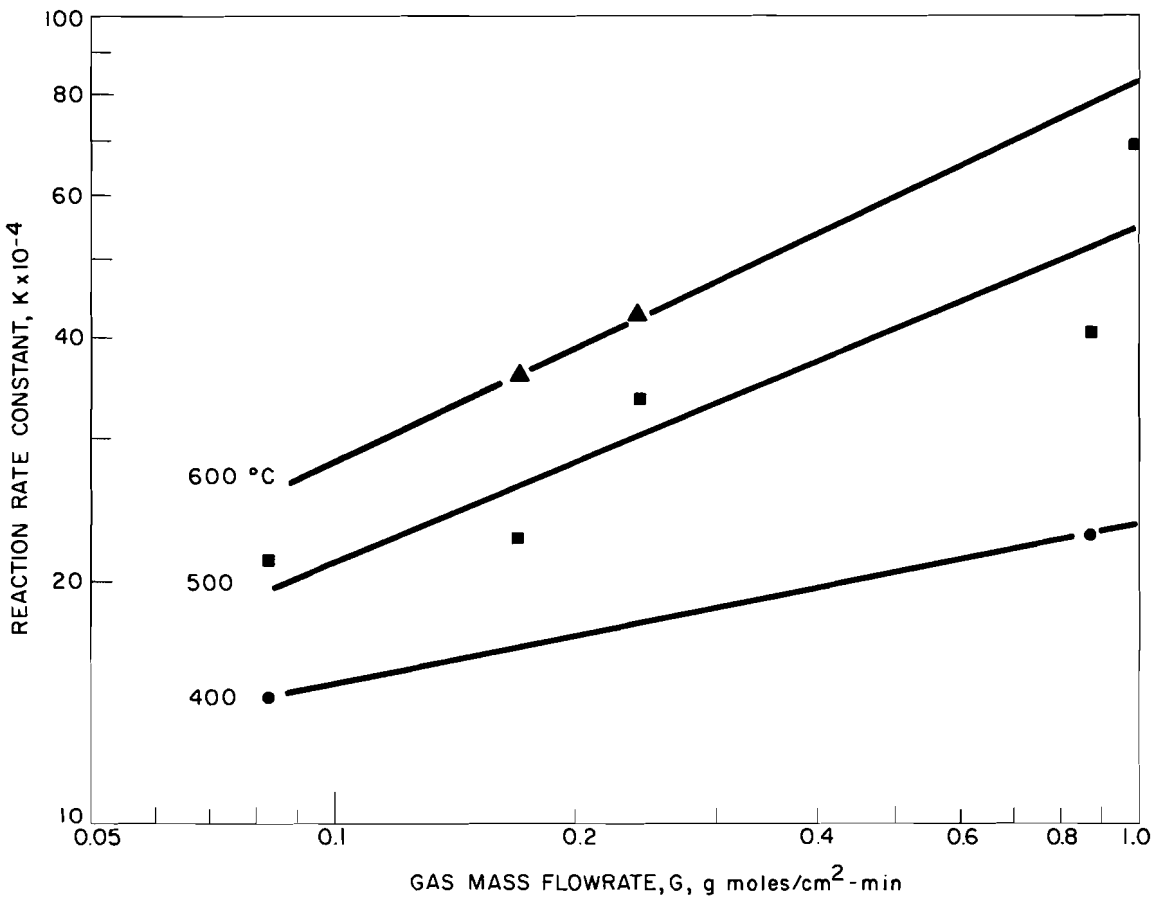

Fig. 2.3. Log reaction rate constant for catylzed reaction, $H_2 + 1/2\ O_2 = H_2O$, vs log mass flowrate.

UNCLASSIFIED
ORNL-LR-DWG 64270

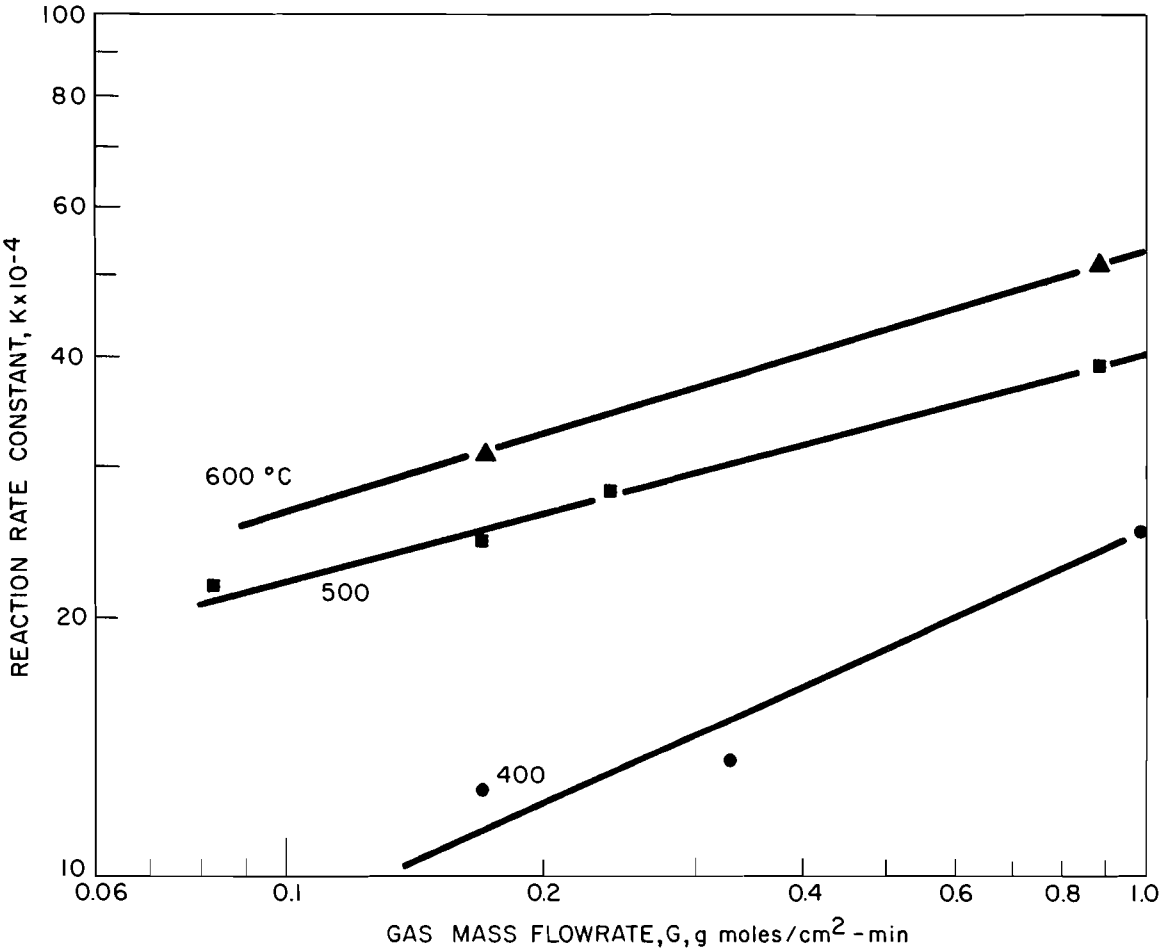

Fig. 2.4. Log reaction rate constant for catalyzed reaction, $CO + 1/2\ O_2 = CO_2$, vs log mass flowrate.

UNCLASSIFIED
ORNL-LR-DWG 64271

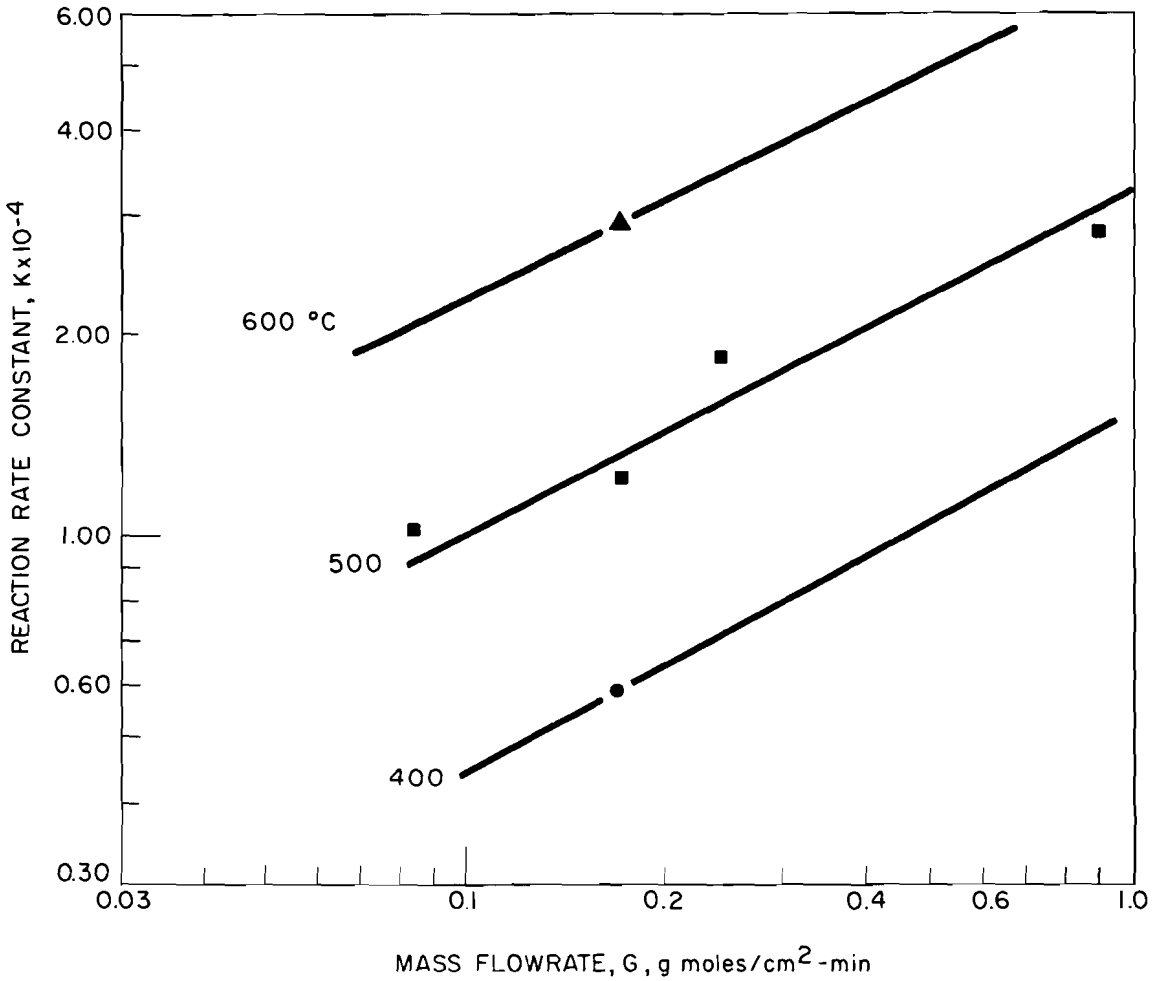

Fig. 2.5. Log reaction rate constant vs log mass flowrate for catalyzed reaction, $CH_4 + 2\,O_2 = CO_2 + 2H_2O$.

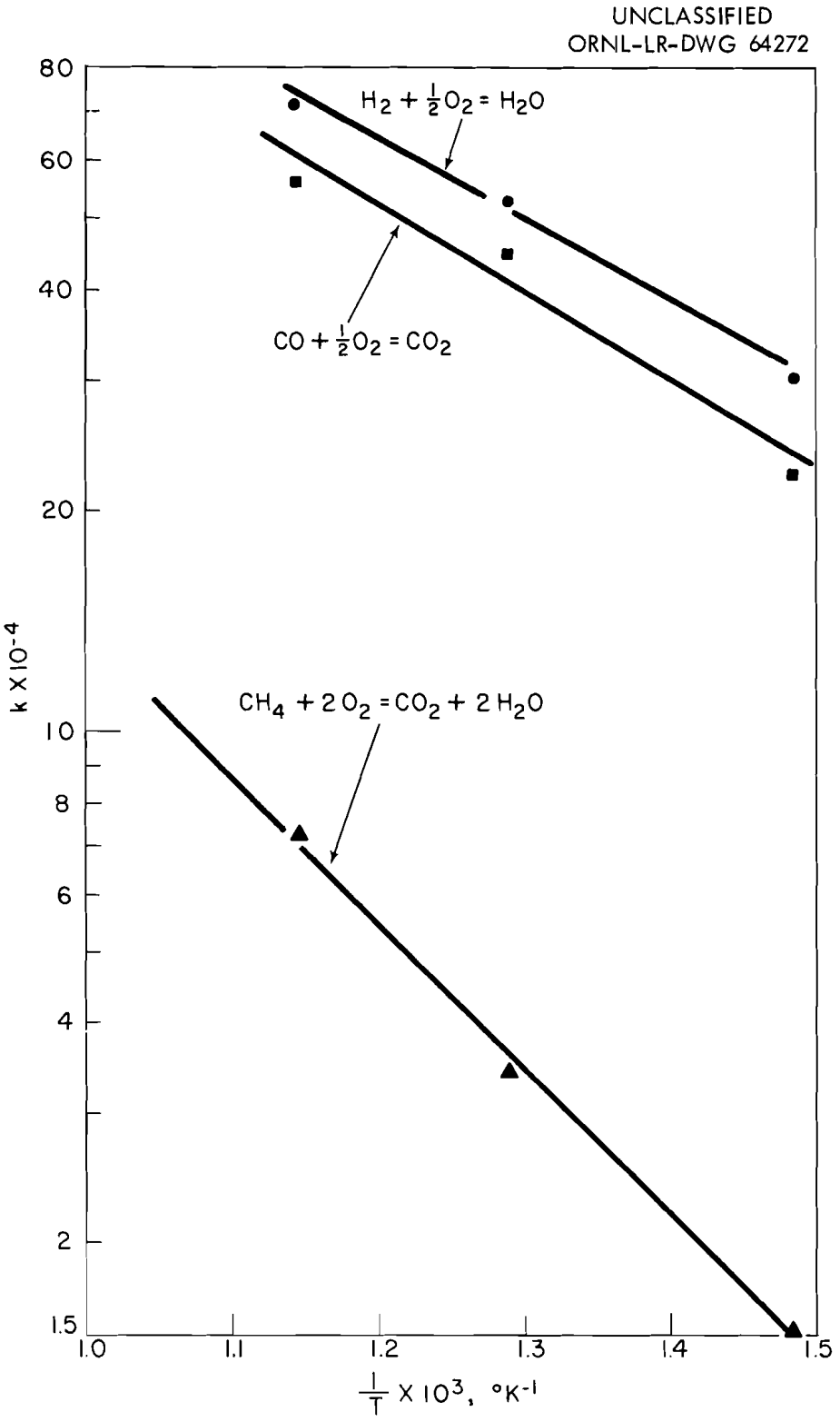

Fig. 2.6. Arrhenius plots of the rate constants for the catalyzed reactions of H_2, CO, and CH_4 with O_2 in a flowing stream of helium at 300 psia.

For carbon monoxide,

$$k = 1.73 \times 10^{6} e^{-2400/RT} \tag{10}$$

For methane,

$$k = 4.08 \times 10^{5} e^{-3950/RT} \tag{11}$$

Putting the values for Θ and the expressions for k in eqs. (1) and (6) gives expressions for the apparent reaction rates,

For hydrogen,

$$r_H = 1.95 \times 10^{6} e^{-2200/RT} G^{0.37} y_H y_O \tag{12}$$

For carbon monoxide,

$$r_H = 1.73 \times 10^{6} e^{-2400/RT} G^{0.34} y_C y_O \tag{13}$$

For methane,

$$r_{CH} = 4.08 \times 10^{5} e^{-3950/RT} G^{0.51} y_{CH} y_O \tag{14}$$

Simultaneous Oxidation of Hydrogen, Carbon Monoxide, and Methane. The three series of tests made with simultaneous oxidation of the three contaminants showed that the preference of oxidation in the catalytic bed was hydrogen first, carbon monoxide second, and methane last. That is, the major portion of the hydrogen was oxidized prior to significant carbon monoxide or methane oxidation and the major portion of the carbon monoxide was oxidized prior to significant methane oxidation. Although these effects were not quantitative, for a conservative reactor design it should be assumed that the first portion or zone of the catalytic bed will be utilized for hydrogen oxidation by the total amount of oxygen available. The second zone for carbon monoxide oxidation by the total remaining oxygen, and the final portion of the oxidizer will oxidize the methane with the oxygen remaining after both hydrogen and carbon monoxide oxidation.

Reactor Design Equations. One of the main purposes of this work was to establish necessary design equations for evaluation of the EGCR catalytic oxidizer. The design equations can be developed by rearranging eqs. (3), (4), and (5) and incorporating eqs. (9), (10), and (11) for the apparent rate constants. The resulting design equations are:

For hydrogen,

$$V_H = \frac{5.12 \times 10^{-7} e^{2200/RT}}{G^{0.37}\left(y_{H_o} - 2y_{O_o}\right)} \ln \frac{y_{H_f}\, y_{O_o}}{y_{H_o}\, y_{O_f}} \tag{15}$$

For carbon monoxide,

$$V_C = \frac{5.77 \times 10^{-7} F e^{2400/RT}}{G^{0.34}\left(y_{C_o} - 2y_{O_o}\right)} \ln \frac{y_{C_f}\, y_{O_o}}{y_{C_o}\, y_{O_f}} \tag{16}$$

For methane,

$$V_{CH} = \frac{2.45 \times 10^{-6} F e^{3950/RT}}{G^{0.51}\left(2y_{CH_o} - y_{O_o}\right)} \ln \frac{y_{CH_f}\, y_{O_o}}{y_{CH_o}\, y_{O_f}} \tag{17}$$

To evaluate an existing oxidizer, eqs. (15) and (16) can be used to establish the necessary oxidizer volume for the H_2 and CO oxidation and the remaining volume will be used to oxidize the CH_4. Equation (17) can be rearranged to give a value of the CH_4 concentration when the catalyst volume to be used will be the remaining effective volume (V_{CH} = total volume - V_H - V_C):

$$y_{CH_f} = \frac{y_{CH_o}\, y_{O_f}}{y_{O_o}} \exp\left[\frac{4.08 \times 10^5 V_{CH} G^{0.51} e^{3950/RT}\left(2y_{CH_o} - y_{O_o}\right)}{F}\right] \tag{18}$$

where

V = volume of catalyst remaining for the methane oxidation, cc

It should be noted that when simultaneous oxidation of two or more contaminants is contemplated, necessary reactor volumes are additive for each contaminant and the oxygen mole fraction to be used is the total unused oxygen in the gas stream.

Reaction-rate-controlling Mechanism. Although the tests made in this study were not exhaustive enough to establish the rate-controlling mechanism, there was definite indication that mass transfer of both the contaminant and oxygen to the reaction site from the bulk gas stream contributed to the reaction rate control.

This is indicated by the dependence of reaction rate on the mass flow rate and by the low activation energies of the reaction rate constant.

EGCR Application of Oxidizer. The design criteria established for the EGCR oxidizer[1-3] plus addition of some capacity for methane oxidation would give the following gas impurity levels for the EGCR oxidizer:

Contaminant	Gas, vol % Impure	Purified
H_2 (ref 1,2)	2.3	< 0.1
CO (ref 1,2)	2.3	< 0.1
CH_4	0.01	

(There are no requirements for methane oxidation in EGCR design specification, but it is felt that a realistic design should include provisions for this contaminant. There are no requirements for O_2 contamination from the oxidizer, but it should be maintained as low as possible.)

With these criteria and the reactor design equations and assuming that the mass flow rate will be 0.82 g mole/cm^2-min, and the temperature 650°C, for H_2 and CO oxidation only, it was determined that the oxygen concentration in the oxidizer effluent would have to be somewhat higher than 10 ppm but less than 100 ppm. If significant methane oxidation is needed, the effluent oxygen concentration would have to be greater than 100 ppm.

If the design specifications for contaminant content are realistic, then the available catalytic oxidizer is not sufficient to oxidize all contamination, including methane, without significant oxygen contamination of the coolant.

It is recommended that the following points be considered:

1. The oxidizer should be operated at as high a temperature as possible.

2. The design specifications for contamination levels should be re-investigated.

3. If it is necessary to maintain low O_2 content in the oxidizer effluent (less than 10 ppm), with the contamination levels specified, if capacity for methane oxidation is necessary, or if a lower operating temperature must be used (< 650°C), then a larger oxidizer should be procured with design based on the design equations given in this report.

4. If contamination levels, including O_2 contamination, must be maintained significantly lower than the above specifications, oxidation by fixed-bed CuO should be considered.[8,9]

References

1. L. H. Landrum, American Metal Products Co., personal communication, July 6, 1961.

2. F. A. Anderson, "Proposed Helium Purification System for the Experimental Gas-Cooled Reactor (EGCR)," ORNL-2819 (1959).

3. W. L. Albreck, TVA, personal communication, July 5, 1961.

4. M. E. Whatley et al., "Unit Operations Section Monthly Progress Report, February 1960," ORNL CF 60-2-56.

5. J. M. Smith, "Chemical Engineering Kinetics," McGraw-Hill Book Co., New York, 1956.

6. S. Waller, "Analysis of Kinetic Data for Heterogeneous Reactions," J.A.I.Ch.E., 2: 39 (1956).

7. C. D. Scott, "Kinetics of the Catalyzed Oxidation of Hydrogen, Carbon Monoxide, and Methane by Oxygen in a Flowing Stream of Helium," ORNL-3043 (1961).

8. C. D. Scott, "Oxidation of Hydrogen and Carbon Monoxide in Helium by Use of CuO. I. Preliminary Results," ORNL CF 60-7-26.

9. C. D. Scott, "Removal of Hydrogen, Carbon Monoxide, and Methand from Gas Cooled Reactor Helium Coolants," ORNL-TM-20 (1961).

3.0 POWER REACTOR FUEL PROCESSING

C. D. Watson

3.1 Shear and Leach - B. C. Finney

A shear and leach program to determine the economic and technological feasibility of continuously leaching the core material (UO_2 or UO_2-ThO_2) from relatively short sections (1-in. long) of fuel elements produced by shearing is continuing. This processing method enjoys the apparent advantage of recovering fissile and fertile material from spent power reactor fuel elements without dissolution of the inert jacketing and end adaptors. These unfueled portions are stored directly in a minimum volume as a solid waste. A "cold" shear and leach complex consisting of a shear, conveyor-feeder, and leacher is being evaluated prior to "hot" runs.

Shear. A method of feeding and holding a fuel assembly during shearing appears to be acceptable from initial field tests. Spring loading the inner gag hydraulic cylinder (Figure 3.1) of the shear to reduce the force required to move the gag at zero hydraulic pressure from ~800 lbs to ~100 lbs measured at the face of the gag permitted the successful shearing of a Mark I porcelain filled prototype fuel assembly to within 1-1/2 in. of the end (Figure 3.2). The length of the terminal cut is determined by the thickness of the inner gag because the feed mechanism pusher arm head cannot move inside the inner gag. The fuel assembly was successfully moved forward after each cut by retracting the outer gag, reducing the inner gag hydraulic pressure to zero, and using the feed mechanism hydraulic pressure (~65 psig water) to move the fuel assembly through the inner gag against a stop which sets the cut at 1 in.

Preliminary tests made using a stepped moving blade to shear into the flat side of a Mark I prototype fuel assembly indicate that discrete pieces are produced; however, the sheared face of the bundle is not as compact as when shearing across the diagonal, and drag back of tube occurs when the movable blade is retracted (Figure 3.3). Scouting tests will be made shearing into the flat side of the bundle using a flat blade rather than the stepped blade.

The force required to shear a highly embrittled carburized (~1.7-2.7% C) porcelain-filled Mark I prototype fuel assemblies (Figure 3.4) is ~25 tons compared to ~50 tons for the ductile cladding. The conditions for carburization are:

	Gas	Flow Rate, cfh	Time, hr	Furnace Temp.
1.	He	20	~2.5	Room to 1100°C
2.	H_2	40	2.75	1100°C
	CH_4	~35		
3.	He	20	1.0	1100°C
4	He	20	Until cool (overnight)	

UNCLASSIFIED
PHOTO 56099

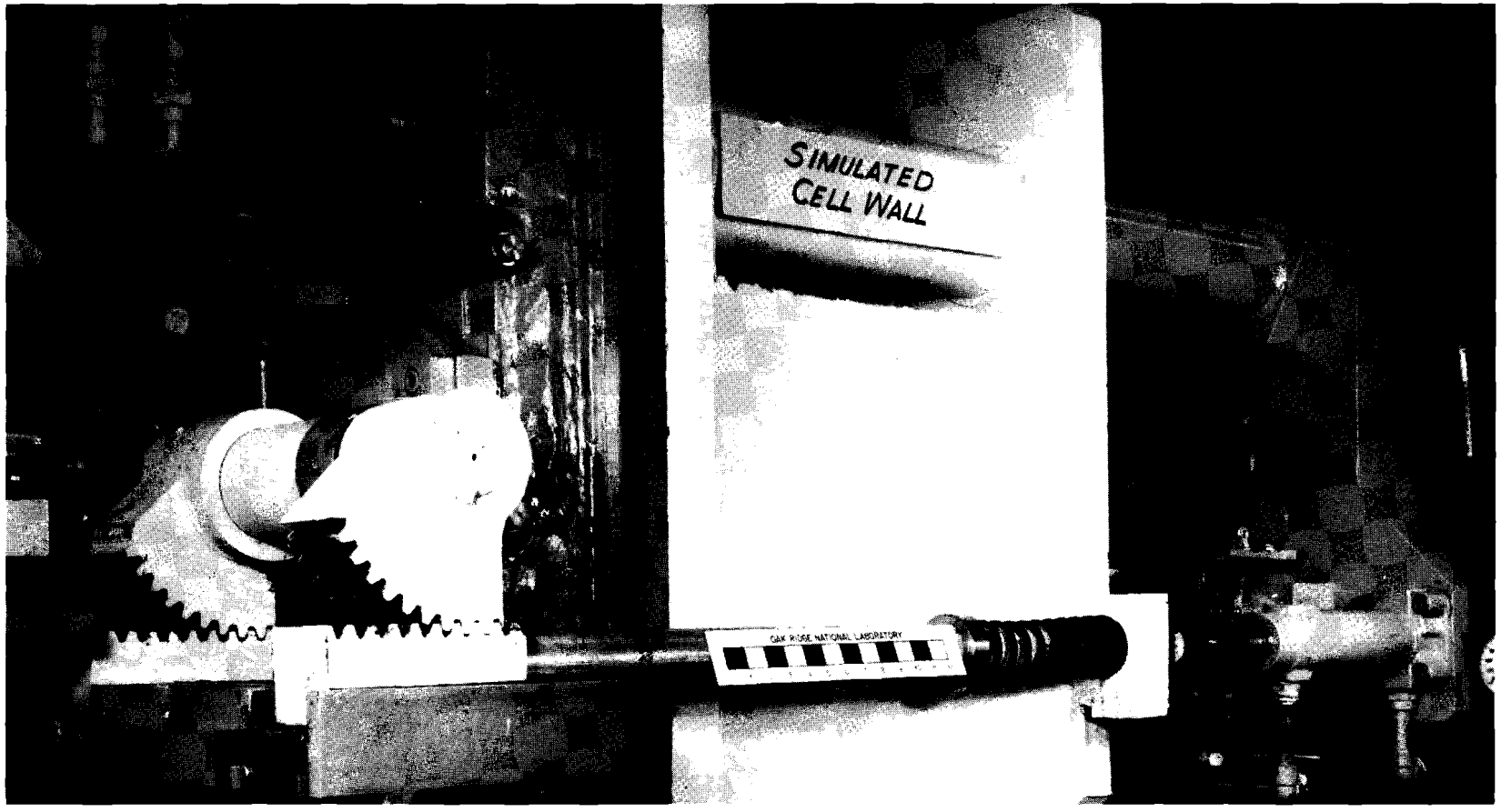

Fig. 3.1. 250-ton prototype shear inner gag hydraulic (oil) mechanism showing position of spring to reduce force required to open gag.

UNCLASSIFIED
PHOTO 56094

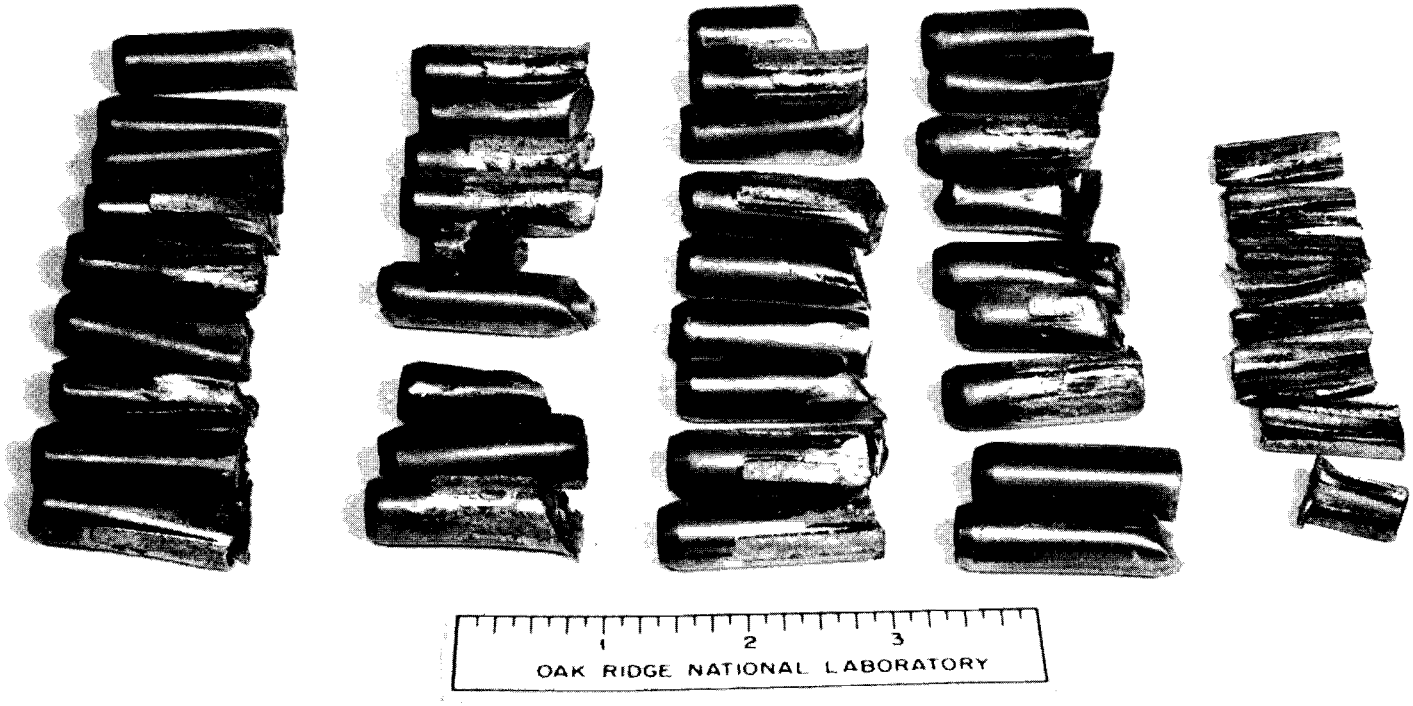

Fig. 3.2. End pieces of porcelain filled ORNL Mark I fuel assembly sheared with stepped movable blade using spring loaded inner gag to hold assembly.

UNCLASSIFIED
PHOTO 56203

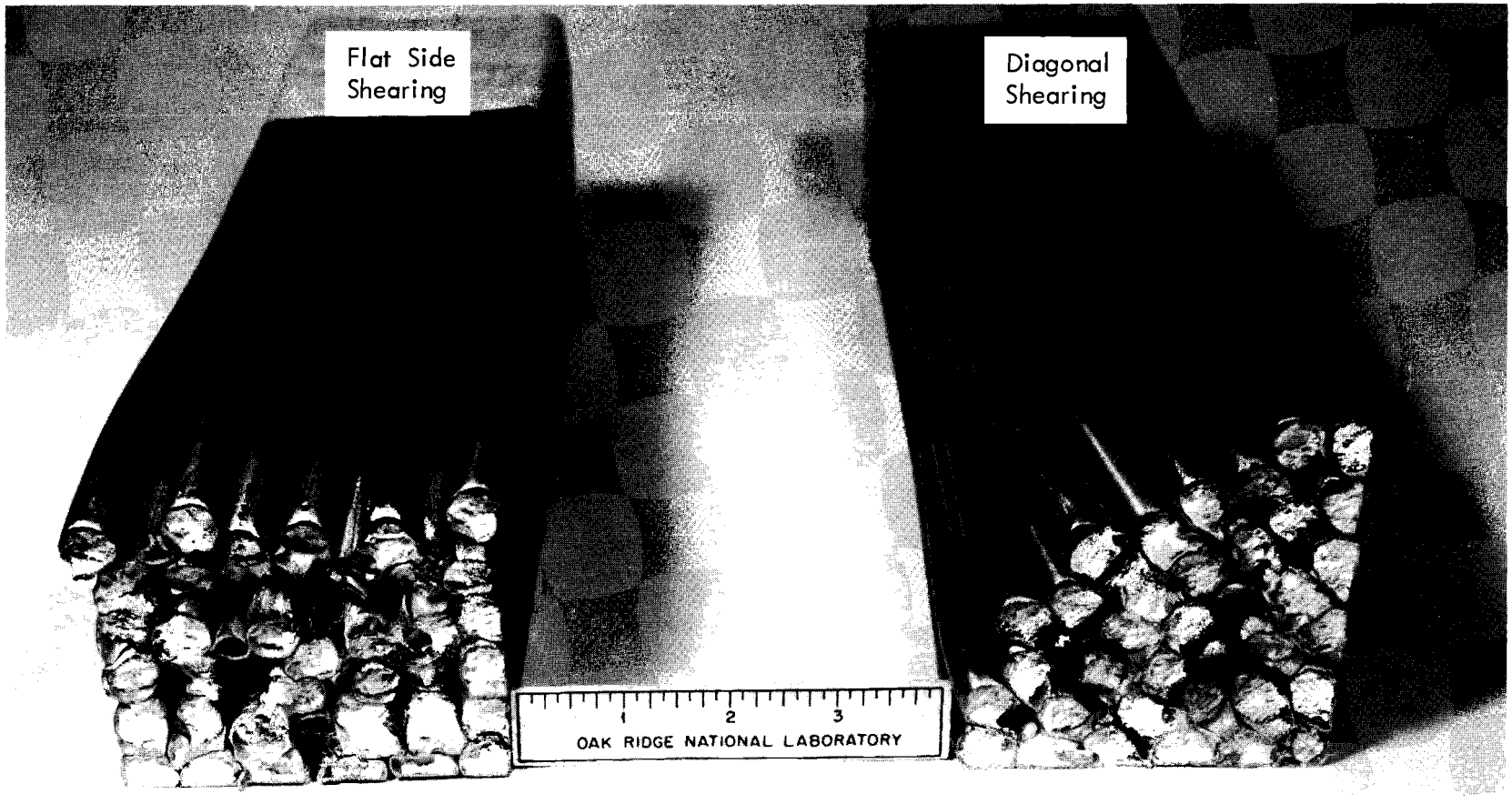

Fig. 3.3. Shape of bundle force when shearing into the flat side and across the diagonal at a double row of ferrules of a porcelain filled ORNL Mark I prototype fuel assembly using a stepped blade.

UNCLASSIFIED
PHOTO 56100

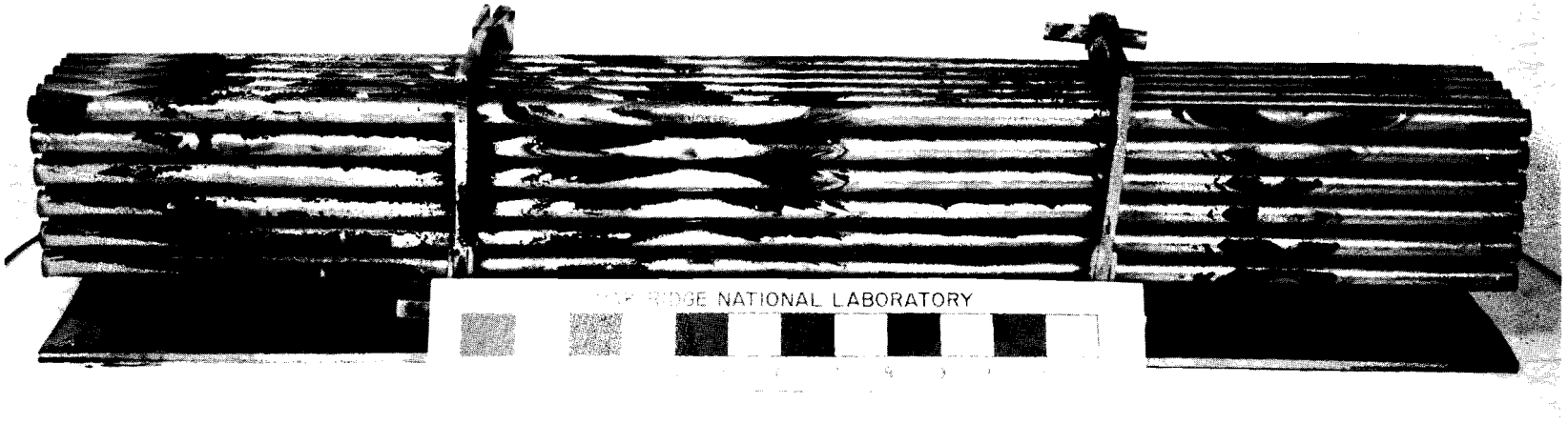

Fig. 3.4. Section of carburized (1.79-2.62% C) porcelain filled ORNL Mark I fuel assembly.

The cladding shattered badly during shearing exposing more of the porcelain than when shearing ductile cladding (Figure 3.5 and Table 3.1). Both the carburized cladding and porcelain are very brittle and consequently some attrition is encountered during sizing.

Four pieces of the carburized cladding weighing 16.8 g lost 2.3 g when placed in boiling 8 M HNO_3 for 4 hrs. After exposure to acid the pieces were coated with a thin bright layer which easily flaked off.

Leacher. Further testing of the leacher rotary drum indicates that a 2.25 liter bulk volume of sheared fuel assembly sections, equivalent to 6.5 kg of UO_2 in a Mark I, is the maximum batch size that can be adequately covered with the leachant acid. The leacher operated satisfactorily conveying sheared sections of a porcelain filled fuel assembly against counterflowing water used to simulate acid. A baffle was welded in the discharge end of the leacher to insure the proper discharge of a complete batch of fuel assembly sections each revolution. The manual and automatic controls operated satisfactorily.

3.2 SRE Dejacketing Studies - G. A. West

Demonstration of the mechanical dejacketing of NaK bonded stainless steel-jacketed SRE Core I fuel burned to ~675 mwd/ton and cooled about 2 years is complete. All fuel received was successfully dejacketed by one of three methods. A total of 1786.65 kg of uranium consisting of 2,165 slugs, 0.75-in.-OD x 6-in.-long (12 slugs per fuel rod), were dejacketed; 16% of which were hydraulically flushed from the tubular jackets, 73.5% were forced out with a jackscrew and 10.5% were cut at the slug junctures, the jacket slit and pried from the slug.

The final experimental production rate, not including down time for repairs, was 5.1 kg U/hr, attaining a maximum of 9.2 kg U/hr (Figure 3.6). The average processing rate was 2 kg U/hr when including total time (operating, maintenance, and equipment changes). Approximately 218 hr were required to rebuild and maintain the system for disposal of NaK which accounts for ~39% of the total down time.

A total of ten SRE stainless steel fuel jackets were dissolved in aqua regia. Batch dissolutions of one jacket each were made in 2 M HCl-5 M HNO_3 and 3 M HCl-4 M HNO_3. The irradiated stainless steel jackets were completely dissolved in 3 out of 5 batch dissolutions producing a product loading of 50 g stainless steel/liter where the molar ratio of Cl^- to stainless steel was 3.5 to 1 (3 M HCl-4 M HNO_3). The classical 2 M HCl-5 M HNO_3 solutions at a 2.35 to 1 Cl^- to stainless steel ratio did not completely dissolve the jackets and a cleanup run was always required. Analysis of the product solutions show a negligible uranium loss from the mechanical dejacketing operation (Table 3.2). Low concentrations of uranium, 0.0001 to 0.0041 mg/ml or 0.1 to 4.6 mg U/mole of stainless steel, and Pu at 108 to 1.1 x 10^3 counts/min/ml were measured. Carbon, of up to 0.2%, was found in 7 of the 10 product solutions. A gamma spectrometric scan of the dissolved jacket showed only trace quantities of fission products originating from the core fuel. Analysis of a powdery deposit scraped

UNCLASSIFIED
PHOTO 56204

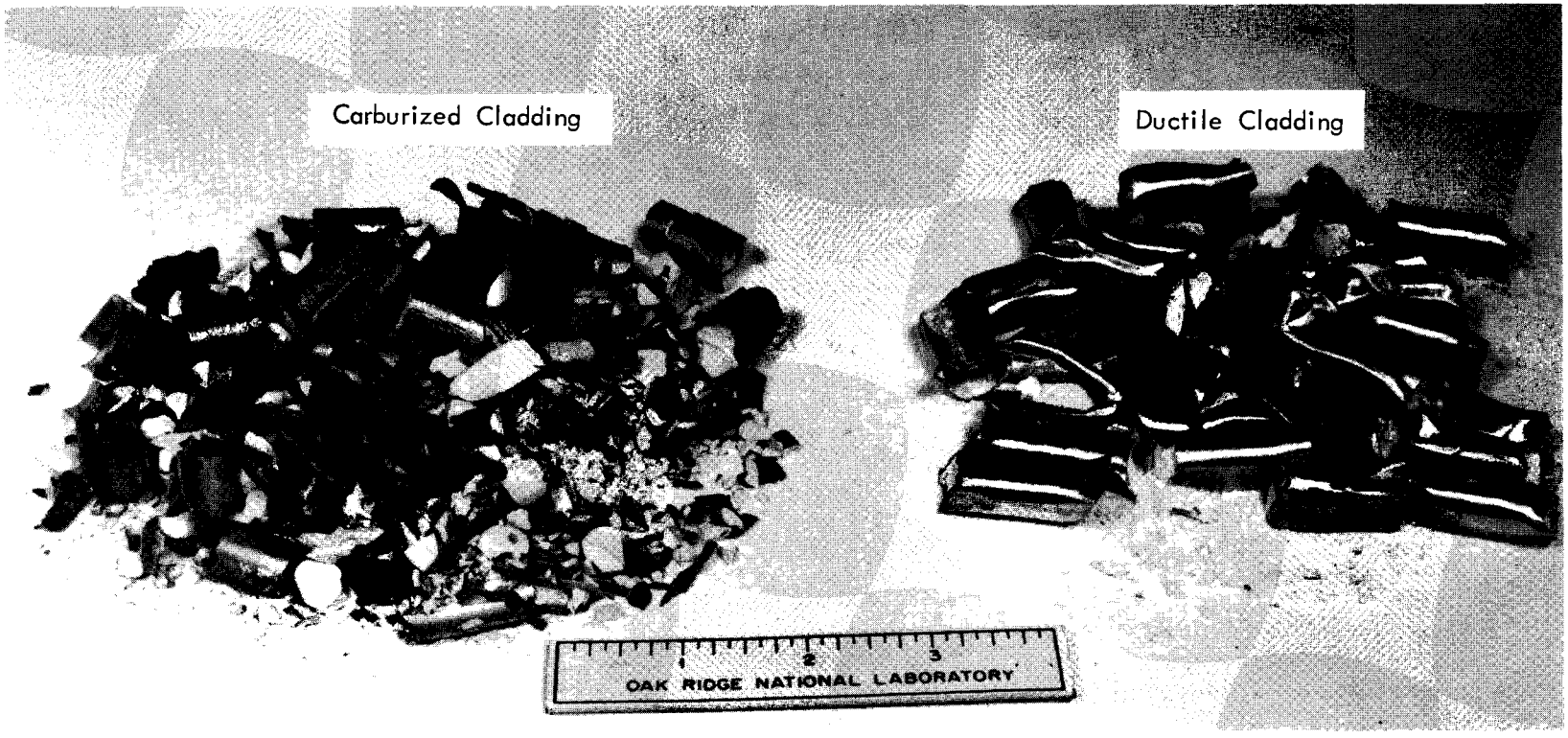

Fig. 3.5. Comparison of single cut made on carburized and ductile porcelain filled ORNL Mark I prototype fuel assemblies.

Table 3.1. Particle Size Distribution of Cut Made on Carburized and Ductile Mark I Fuel Assemblies

Particle Size, microns	Carburized		Ductile	
	Porcelain Wt, g	Stainless Steel Wt, g	Porcelain Wt, g	Stainless Steel Wt, g
+9520	107.1	196.3	487.8 (porc. + SS)	31.4 (ferrules)
-9520 +4760	61.1	64.6	-	-
-4760 +2000	32.6	42.2	1.07	2.64
-2000 +1190	13.8	8.4	3.26	0.48
-1190 +590	10.8	2.7	7.21	0.41
-590 +297	6.0	0.9	7.95	0.37
-297 +149	3.5	0.4	6.57	0.28
-149 +74	2.0	0.15	4.13	0.26
-74 +44	1.1	0.09	2.47	0.21
-44	1.0	0.05	3.05	0.03

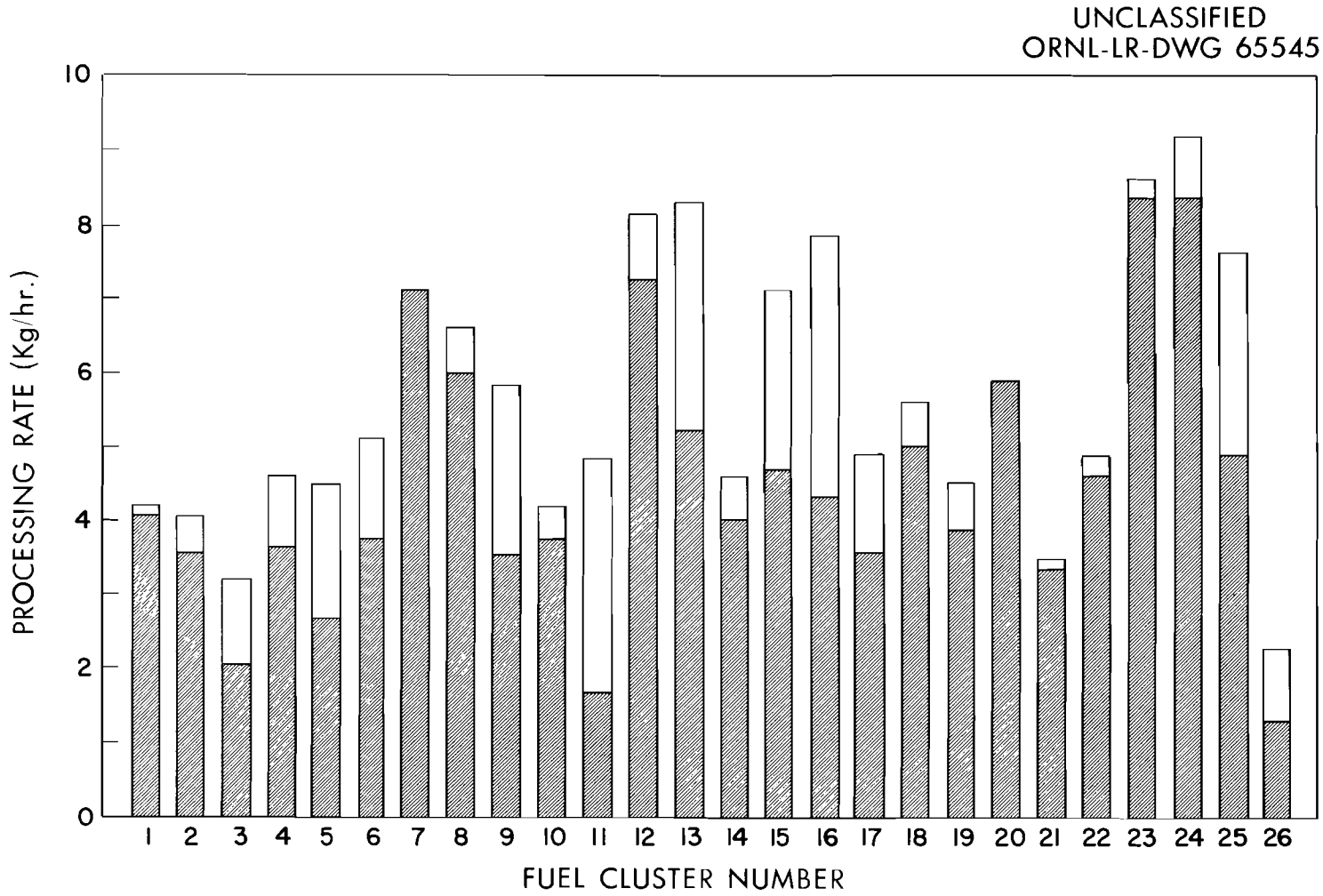

Fig. 3.6. Mechanical dejacketing of SRE Core I fuel.

FUEL: 12 U slugs per rod, 0.750'' OD × 6'' long, 10 mil NaK bond, in 304 s/s jackets, 0.790'' OD, 10 mil wall × - 8 ft. long. 7 rods per element.

NOTE: (1) Peak of unshaded portion = Dejacketing rate not including down time.
(2) Peak of shaded portion = Dejacketing rate including all down time for maintenance and repairs.

Table 3.2. Batch Dissolution of Irradiated SRE Core I Fuel Jackets

Jackets: 304 SS, 10 mil wall, 280 g/batch
Conditions: (1) Boiling aqua regia, 6 liter volumes
(2) Runs 1 through 4, 2 M HCl-5 M HNO_3
Run 5, 2.5 M HCl-5 M HNO_3
Runs 6 through 10, 3 M HCl-5 M HNO_3

	Run No.									
	1	2	3	4	5	6	7	8	9	10
U (g/liter)	0.0015	0.0013	0.0002	0.0036	0.0015	0.0022	0.0020	0.0021	0.0013	0.0020
Pu (c/m/ml)	248	108	224	1.1×10^3	148	144	240	336	160	208
Cr (%)	17.5	19.7	21.6	17.5	14	14.2	13.6	14.5	16.3	16.4
C (%)	0.05	0	0	0.015	0.217	0	0.05	0.04	0.024	0.009
Product, H^+ (N)	3.75	4.07	4.67	3.86	3.06	3.75	4.42	4.03	3.94	3.63
Product, Cl^- (N)	1.59	1.73	1.8	1.71	1.7	2.76	2.76	1.08	2.88	2.74
Gross* γ, (c/m/ml)	6.6×10^7	4.64×10^7	4.42×10^7	1.52×10^8	7.0×10^7	5.16×10^7	6.4×10^7	1.06×10^8	6.74×10^7	5.40×10^7
Co^{58-60}, γ (c/m/ml)	6×10^7	-	4.4×10^7	1.21×10^8	6.9×10^7	5.0×10^7	6.3×10^7	1.02×10^8	6.6×10^7	5.35×10^7
Sr^{89-90}, γ (c/m/ml)	7.7×10^4	-	4.6×10^4	1.3×10^5	4.9×10^4	3×10^4	3.4×10^4	6.9×10^4	1.2×10^5	4.4×10^4
Cs^{137}, γ (c/m/ml)	$< 3 \times 10^4$	-	7.5×10^3	$< 3 \times 10^4$	1.4×10^4	1.4×10^4	2.4×10^4	1.4×10^4	9.3×10^3	9.3×10^3
Ru^{106}, β (c/m/ml)	2.2×10^3	-	8.9×10^3	3.6×10^4	1.3×10^4	7.2×10^3	1.4×10^4	4.3×10^4	1.1×10^4	1.5×10^4
Zr^{95}, γ (c/m/ml)	$< 1 \times 10^3$	-	$< 1 \times 10^3$	3.9×10^4	$< 1 \times 10^3$	$< 1 \times 10^3$	$< 1 \times 10^3$	1.6×10^3	1.2×10^3	2.6×10^3

* FP analysis at ± 10%.

from the exterior surface of the jackets showed only stainless steel constituents and no carbon or other products that would contribute to the embrittled condition of the irradiated jackets. Samples of jackets are undergoing further metallurgical examinations.

Equipment removal and decontamination of the segmenting cell is ~90% complete. Personnel exposures during the decontamination phase has averaged only 57 mr/week. The highest background readings were 10 rads/hr, measured in the vicinity of the abrasive disc cut-off saw.

3.3 U-C Fuel Processing - B. A. Hannaford

Recovery of uranium and thorium from graphite fuels by a "semicontinuous" method appears to offer advantages over batch processing for fuels amenable to the nitric acid flowsheets: 90% HNO_3 and grind-leach. To help define a semicontinuous 90% HNO_3 flowsheet gross measurements were made of (1) the rate at which uranium is solubilized in a batch contact, and (2) the rate at which dissolved uranium is washed from the graphite by water. In another experiment the degree of preliminary mechanical crushing was shown to affect uranium loss to the graphite residue.

Undissolved Uranium vs Acid Contact Time. Small samples of 2.6% U-graphite fuel digested in 90% HNO_3 at 60°C showed a very slow decrease in undissolved U concentrations for times longer than 30 min. Analysis of leach solutions and thoroughly washed residues are shown in Table 3.3.

Washing Dissolved Uranium from Acid-leached Fuel. In order to determine the degree to which the rate of uranium removal by wash water is dependent on residue particle size, acid-leached fuel was separated into two size fractions and washed in water for varying lengths of time. Results are summarized in Table 3.4. Because of the very considerable scatter of the data it was not possible to calculate the concentration of dissolved uranium remaining in the washed residue. However, the results indicate that elution of uranium is very rapid during the washing process, since the total residual uranium concentration did not change significantly beyond the shortest wash times employed - 0.5 and 1.0 min.

Uranium Loss vs Degree of Mechanical Crushing. Since previous semicontinuous leaching experiments had indicated the possibility that uranium recovery was actually decreased by excessive mechanical crushing prior to leaching (Unit Operations monthly report, October 1961), a run was made in which the fuel was jaw-crushed to yield -2 mesh feed with a minimum of fines. The resulting uranium loss was not only lower (by a factor of 4) than sustained for the more finely divided fuel, but the sieved residue fractions also exhibited an inverse relationship between particle size and residual uranium (Table 3.5).

Table 3.3. Undissolved Uranium vs Acid Contact Time

Weight of graphite fuel samples: ~0.6-0.8 g.
Acid/Fuel ratio: 13-17 ml/g

Digestion Time, hr	(H^+) Initial, M	(H^+) Final, M	U in Residue, ppm
0.5	21.3	20.0	705
1.5	21.3	20.3	610
6.0	21.3	19.8	540

Table 3.4. Residual Uranium Concentration vs Particle Size, Wash Time

2.6% graphite fuel digested in 90% HNO_3 at 60°C for 6 hrs. Size separation by sedimentation in mother liquor. Wash water at room temperature.

Stoke's Dia, μ	Wash Time, min	Total Residual (U), ppm	Stoke's Dia, μ	Wash Time, min	Total Residual (U), ppm
575-680	0	3125 ± 91	< 55	0	4149
575-700	1	520 ± 11	< 55	0.5	619
575-660	2	599 ± 12	< 55	1	728
575-680	10	443 ± 1	< 55	2	549
575-750	60	510	< 55	10	719

Table 3.5. Results of Semicontinuous Leach Run 108

Fuel size, as charged: 100% < 2 mesh, 27% < 12 mesh. Leaching conditions same as for run 105: Batch leach in 90% HNO_3 at 60°C for 2 hrs, continuous flow of acid at rate of 0.81 bed volumes/hr for 4 hrs, final water wash to clear effluent. Fuel composition: 2.6% U

	Run 108 Uranium conc., ppm	Run 105 (from October Monthly) Uranium conc., ppm
Composite residue	98 ± 8 = 0.37% loss	417 ± 43
4/12 mesh residue	119 ± 3	
25/50 mesh residue	111 ± 1	
140/325 mesh residue	301 ± 14	
1.5 cm "lump"	107 ± 15	
"fines" from top of bed	167 ± 2	

4.0 REACTOR EVALUATION STUDIES

J. C. Suddath

4.1 Heat Transfer from Spent Fuel Elements during Shipping - J. S. Watson

Experimental measurements and attempted predictions of temperatures within mock spent reactor fuel elements in a simulated carrier have been continued. The most notable development has been in obtaining better predictions of the observed temperatures. The analysis of the heat transfer within the fuel and cask has thus far been limited to radiation. This is apparently a major method of heat transfer in air filled casks with relatively high heat generation rates. The effects of convection could best be deduced if the thermal fluxes due to radiation were accurately evaluated.

The previous work has all been based upon diffuse radiation and reflection. The configuration factors for diffuse radiation between the tubes were calculated numerically and the radiation factors (including the effects of emissivity) were estimated in an apparently conservative manner. The wall of the cask was simulated in the calculations by assuming that the bundle was surrounded by two extra rows of tubes maintained at the wall temperature. Calculations of the expected temperature distribution in the bundle were made assuming that all heat transfer was by radiation. The calculated results gave a very good approximation of the center tube temperatures, but the temperatures predicted near the outside of the bundle were very often considerably below those measured experimentally. Apparently the simulated wall gave much too optimistic results and predicted radial fluxes notably higher than the total flux due to radiation and connection. The factors for radiation from tube to tube were conservative or at least they predicted that the radiant fluxes for a given temperature distribution within the bundle were less than the total thermal flux. The optimistic simulation of the cask wall and the conservative radiation factors within the bundle apparently tended to cancel in cases of most interest (large bundles with high heat generation rates) and the predicted center tube temperatures were very close to those measured experimentally (within 15°C). This was fortunate and may prove to be a simple but reasonably accurate method of predicting center tube temperatures, but it can not be considered much better than an empirical fit to the data since the temperature distribution in the bundle is notably different from that predicted.

Attempts to correct the calculations both at the wall and within the bundle have been made. Within the bundle, it was considered likely that spectral rather than diffuse radiation and reflection might be a better approximation to the problem. Most materials radiate and reflect in a manner intermediate between that described as diffuse or spectral. It appeared likely, however, that the relatively smooth metal surfaces of interest give more nearly spectral than diffuse properties. Analytical or even numerical methods of obtaining spectral radiation factors for a system as complicated as the tube bundle of interest was considered much too involved, and it appeared more practical to obtain the factors graphically.

The cross sections of the tubes in the bundle were drawn to scale with the proper spacing. Radial lines were drawn from a specific interior tube to represent emerging beams of heat. These were then "reflected" off each tube such that the angles of reflection and incidence were equal. At each reflection, the surface absorbed a fraction ϵ of the incoming radiation and reflected a fraction $1 - \epsilon$. For an emissivity of 0.55, eight reflections were adequate to reduce the beam to an insignificant intensity. Because of the symmetry of the geometry, it was only necessary to consider radiation from a 45° sector of the emitting tube. The emitted beams were drawn every 2-1/2° giving a total of 19 beams to follow. Although all tubes may be expected to receive some fraction of the radiation from the emitted tube, the great bulk went to the adjacent tubes, diagonal tubes, and other tubes adjacent to the diagonal. For the spacing ($S/r = 2$) and emissivity (0.55) used, these three radiation coefficients were 0.1348, 0.0842, and 0.0074, respectively. These values are slightly more optimistic than the approximate diffuse values used previously.

To predict the temperature distribution within the fuel bundles, these values were used for radiation between all tubes within the bundle. However, radiation from the outer row of tubes to the wall was not simulated with two rows of tubes maintained at the wall temperature. When radial emission lines are drawn from the outer row of tubes to the wall, they may be noted to almost always be reflected back to another tube in the outer row. This suggested that the factors for radiation to the wall might be approximated reasonably well by considering emission continual reflection between the wall and the outer half of these tubes. Then F_{iw} would be approximated by

$$F_{iw} = \frac{1}{2\left(\frac{2}{\epsilon} - 1\right)}$$

The corner tubes have more surface exposed to the wall, and the factor was approximated by

$$F_{cw} = \frac{3}{4\left(\frac{2}{\epsilon} - 1\right)}$$

These values were used. The method of calculation (except for previously mentioned factors) was the same as described in the June 1961 Unit Operations Monthly Report. Although new data have been obtained, the same data were used so that the results could be compared (Figures 4.1-4.4). The newer results give worse predictions of the center tube temperatures, but they probably give a much more accurate picture of the effects of radiation in the cask. One would expect the temperatures predicted on the basis of only radiant transfer to be higher than those observed experimentally since some convection and conduction is bound to take place. The newer results give a very good estimate of the temperatures in the outer rows, and are always higher than the measured results.

UNCLASSIFIED
ORNL-LR-DWG 65546

111.1 86.8	118.6 100.0	119.5 125.0 107.2	120.5 128.1 110.3	124 128.1 110.3	123 125.0 107.2	113.5 118.6 100.0	108 111.1 86.8
118.6 100.0	138.2 119.4	127 148.6 130.0	130.0 153.2 134.6	131 153.2 134.6	130 148.6 130.0	117 138.2 119.4	68 118.6 100.0
117 125.0 107.2	128.5 148.6 130.0	135 161.4 142.4	147.5 167.0 147.9	167.0 147.9	161.4 142.4	148.6 130.0	125.0 107.2
117 128.1 110.3	133 153.2 134.6	143 167.0 147.9	173.0 153.8	173.0 153.8	167.0 147.9	153.2 134.6	128.1 110.3
128.1 110.3	153.2 134.6	141 167.0 147.9	144 173.0 153.8	145 173.0 153.8	144 167.0 147.9	98 152.3 134.6	119 128.1 110.3
125.0 107.2	148.6 130.0	137 161.4 142.4	140 167.0 147.9	142 167.0 147.9	138.5 161.4 142.4	128 148.6 130.0	119.5 125.0 107.2
118.6 100.0	138.2 119.4	148.6 130.0	153.2 134.6	130.5 153.2 134.6	124 148.6 130.0	119 138.2 119.4	108.5 118.6 100.0
111.1 86.8	118.6 100.0	125.0 107.2	128.1 110.3	120 128.1 110.3	119 125.0 107.2	108 118.6 100.0	102.5 111.1 86.8

Heat Generation Rate, 0.02158 Watts/Tube-cm

Average Wall Temperature, 53.0°C.

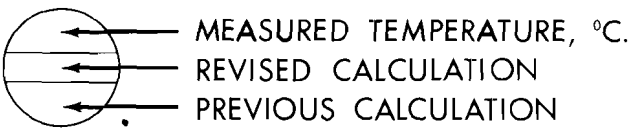

Fig. 4.1. Temperature distribution in a 64 tube vertical bundle at the mid-point.

UNCLASSIFIED
ORNL-LR-DWG 65547

140.88 110.05	150.16 126.94	155 158.11 135.95	156 161.93 139.91	162 161.93 139.91	160 158.11 135.95	148 150.16 126.94	139 140.88 110.05
150.16 126.94	174.28 151.18	166 186.79 164.18	170 192.30 169.83	170.5 192.30 169.83	169.5 186.79 164.18	153 174.28 151.18	83 150.16 126.94
153 158.11 135.95	169 186.79 164.18	176.5 202.08 179.37	192 208.76 186.00	208.76 186.00	202.08 179.37	186.79 164.18	158.11 135.95
154 161.93 139.91	174.5 192.30 169.83	188 208.76 186.00	215.98 193.10	215.98 193.10	208.76 186.00	192.30 169.83	161.93 139.91
161.93 139.91	192.30 169.83	184 208.76 186.00	189 215.98 193.10	190 215.98 193.10	188.5 208.76 186.01	125 192.30 169.83	156 161.93 139.91
158.11 135.95	186.79 164.18	180 202.08 179.37	184 208.76 186.00	186 208.76 186.01	180.5 202.08 179.37	168 186.79 164.18	156 158.11 135.95
150.16 126.94	174.28 151.18	186.79 164.18	192.30 169.83	170.5 192.30 169.83	162 186.79 164.18	155 174.28 151.19	140.5 150.16 126.95
140.88 110.05	150.16 126.94	158.11 135.95	161.93 139.91	157 161.93 139.91	155.5 158.11 135.95	141 150.16 126.95	132 140.88 110.05

Heat Generation Rate, 0.0337 Watts/Tube-cm

Average Wall Temperature, 64.6°C.

MEASURED TEMPERATURE, °C.
REVISED CALCULATION
PREVIOUS CALCULATION

Fig. 4.2. Temperature distribution in a 64 tube vertical bundle at the mid-point.

UNCLASSIFIED
ORNL-LR-DWG 65548

171.30 / 135.00	182.07 / 154.98	196 / 191.25 / 165.53	198 / 195.66 / 170.15	206 / 195.66 / 170.15	203 / 191.25 / 165.53	187 / 182.07 / 154.99	177 / 171.30 / 135.00
182.07 / 154.98	209.83 / 183.24	211 / 224.11 / 198.22	217 / 230.38 / 204.71	218 / 230.38 / 204.71	216 / 224.11 / 198.22	194 / 209.83 / 183.24	98 / 182.07 / 154.99
194 / 191.25 / 165.53	216 / 224.11 / 198.22	226.5 / 241.49 / 215.63	244.5 / 249.05 / 223.20	249.05 / 223.20	241.49 / 215.63	224.11 / 198.22	191.25 / 165.54
197 / 195.66 / 170.15	223 / 230.38 / 204.71	240 / 249.05 / 223.20	257.21 / 231.28	257.21 / 231.28	249.05 / 223.20	230.38 / 204.71	195.66 / 170.15
195.66 / 170.15	230.38 / 204.71	235.5 / 249.05 / 223.20	242 / 257.21 / 231.28	241.5 / 257.21 / 231.28	240.5 / 249.05 / 223.20	160 / 230.38 / 204.71	199 / 195.61 / 170.15
191.25 / 165.53	224.11 / 198.22	230 / 241.49 / 215.63	235 / 249.05 / 223.20	242.5 / 249.05 / 223.20	235 / 241.49 / 215.63	217 / 224.11 / 198.23	200 / 191.25 / 165.54
182.07 / 154.99	209.83 / 183.24	224.11 / 198.22	230.38 / 204.71	218.5 / 230.38 / 204.71	206.5 / 224.11 / 198.23	198 / 209.83 / 183.24	180 / 182.07 / 154.99
171.30 / 135.00	182.07 / 154.99	191.25 / 165.54	195.66 / 170.15	200.5 / 195.66 / 170.15	199 / 191.25 / 165.54	179 / 182.07 / 154.99	168 / 171.30 / 135.00

Heat Generation Rate, 0.04852 Watts/Tube-cm

Average Wall Temperature, 79.4°C.

MEASURED TEMPERATURE, °C.
REVISED CALCULATION
PREVIOUS CALCULATION

Fig. 4.3. Temperature distribution in a 64 tube vertical bundle at the mid-point.

UNCLASSIFIED
ORNL-LR-DWG 65549

80.56 63.50	85.97 72.69	84 90.69 77.76	86 92.99 80.02	88 92.99 80.02	86.5 90.69 77.76	80.5 85.97 72.69	77 80.56 63.50
85.97 72.69	100.53 86.60	89 108.23 94.37	91 111.82 97.81	92 111.82 97.81	91.5 108.33 94.37	82.5 100.53 86.60	52.5 85.97 72.69
83 90.69 77.76	90 108.33 94.37	94 118.08 103.70	102.5 122.40 107.86	122.40 107.86	118.08 103.71	108.33 94.37	90.69 77.76
83 92.99 80.02	93 111.82 97.81	99.5 122.40 107.86	127.12 112.35	127.12 112.35	122.40 107.86	111.82 97.82	92.99 80.03
92.99 80.03	111.82 97.81	98 122.40 107.86	100.5 127.12 112.35	101 127.12 112.35	100 122.40 107.86	71 111.82 97.82	85 92.99 80.03
90.69 77.76	108.33 94.37	96.5 118.08 103.71	98 122.40 107.86	99 122.40 107.86	96.5 118.08 103.71	90 108.33 94.38	85 90.69 77.76
85.97 72.69	100.53 86.60	108.33 94.37	111.82 97.82	92 111.82 97.82	87 111.32 94.38	85 100.53 86.60	78 85.97 72.69
80.56 63.50	85.97 72.69	90.69 77.76	92.99 80.03	85 92.99 80.03	85 90.69 77.76	78 85.97 72.69	74.5 80.56 63.50

Heat Generation Rate, 0.01212 Watts/Tube-cm

Average Wall Temperature, 41.2°C.

MEASURED TEMPERATURE, °C.
REVISED CALCULATION
PREVIOUS CALCULATION

Fig. 4.4. Temperature distribution in a 64 tube vertical bundle at the mid-point.

5.0 VOLATILITY

R. W. Horton

5.1 Zirconium Oxide Dissolution Studies - W. W. Pitt

Dissolution studies of ZrO_2 slabs continued, after several equipment modifications were made to eliminate some problems experienced in previous runs (August 1961 Unit Operations Monthly Progress Report). The rates of ZrO_2 were slightly less than twice that obtained for similar Zr metal runs.

The hydrofluorination system consisted of a 3.5-in.-ID x 24-in. INOR-8 dissolver with an internal off-gas filter (Figure 5.1), an external copper mesh off-gas filter, HF metering equipment, condensers, and HF collectors. Due to limited space, the INOR-8 corrosion specimens were not placed in the dissolver for this series.

Two runs with simulated Zircaloy-2 fuel elements were made to standardize the dissolver. Three runs with ZrO_2 slabs were made at different HF flow rates. All runs were made at ~615°C in a salt with the same initial mole composition: NaF = 22%; LiF = 45%; and ZrF_4 = 32%.

A graphical representation of the Zr metal runs (DO-4 and DO-8) is shown in Figure 5.2. The HF feed rate shown is that obtained by measuring the ΔP across a capillary. The HF discharge rate shown is that obtained by collection of condensed HF over 10 or 20 min time periods. The dissolution rate is that obtained by measuring non-condensable gas evolution. Similar plots for the ZrO_2 runs (DO-5, DO-6, and DO-7) are presented in Figures 5.3, 5.4, and 5.5. Here the dissolution rate was obtained by determining the H_2O evolution over a 10-20 min period.

Table 5.1 is a comparison of averaged dissolution rates obtained by H_2 or H_2O evolution and those obtained by element weight loss. Visual inspection of the ZrO_2 slabs after dissolution indicates that the slabs swell and large sections of the surface spall off. Since this would be a very irregular process, it probably accounts for the wide disagreement in the two methods of determining dissolution rates for ZrO_2.

There appears to be an intermediate compound between $ZrO_2 \rightarrow ZrF_4$ under the conditions of these runs. There are two distinct zones in the element remains after hydrofluorination. The outer one is light gray in color while the inner zone is the same as unreacted slabs. Chemical analysis of the outer zone showed 16.4% F; 19% O; and 64% Zr. This indicates the existence of some intermediate compound such as $ZrOF_2$. A more exhaustive study would be required to establish the mechanism of the dissolution.

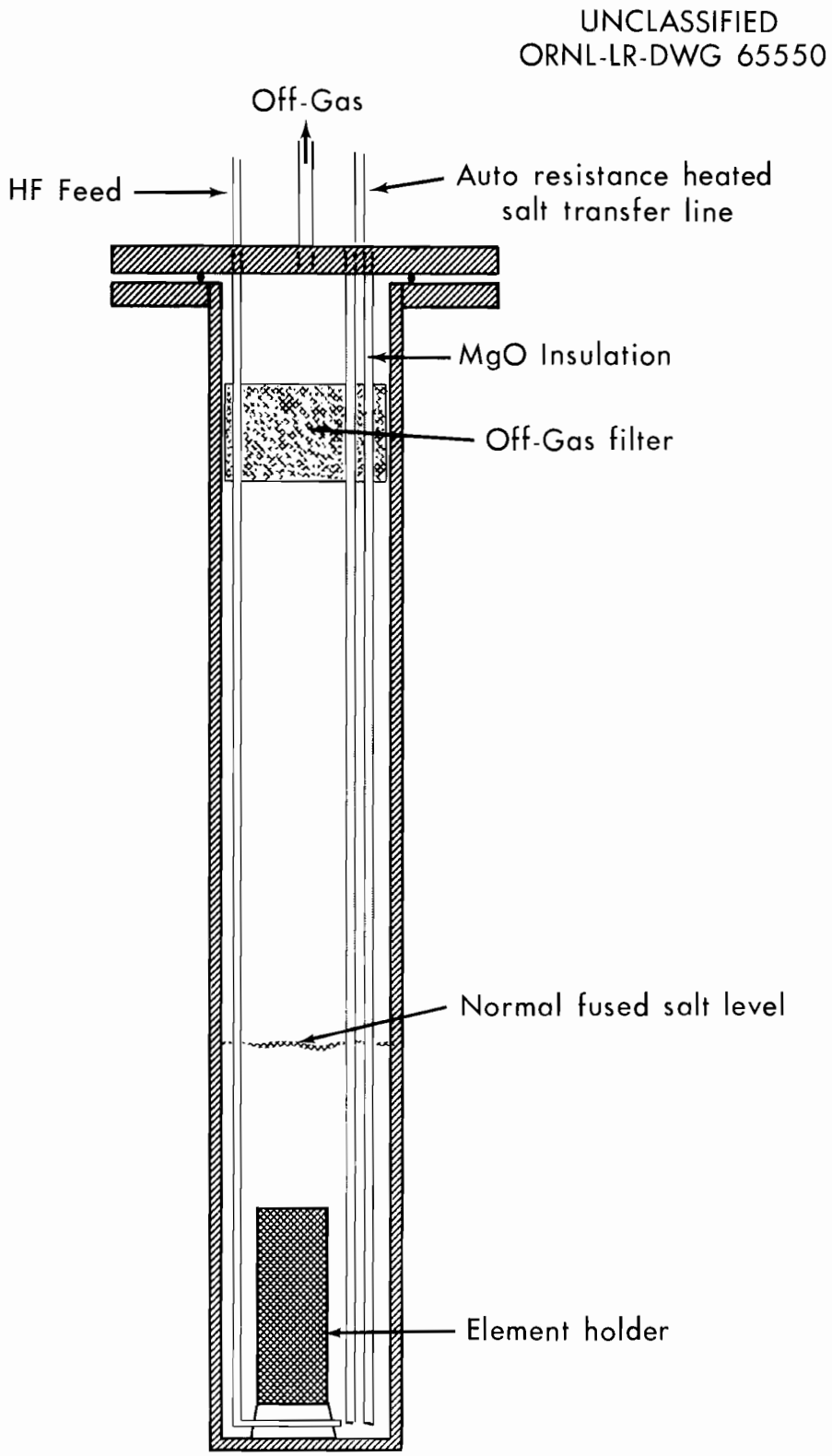

Fig. 5.1. 3.5 in. ID Inor-8 oxide dissolver.

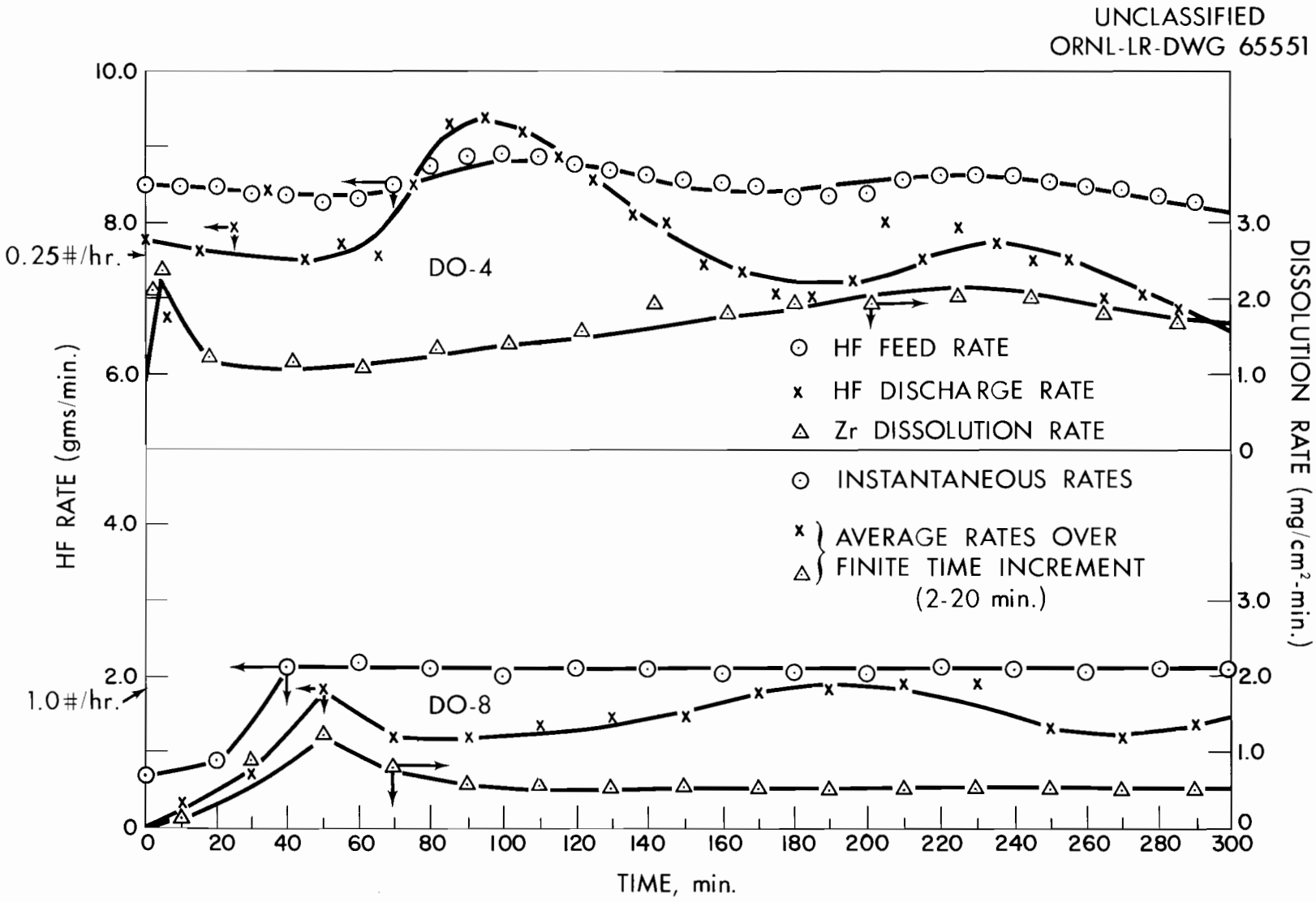

Fig. 5.2. Zirconium metal dissolutions runs DO-4 and DO-8.

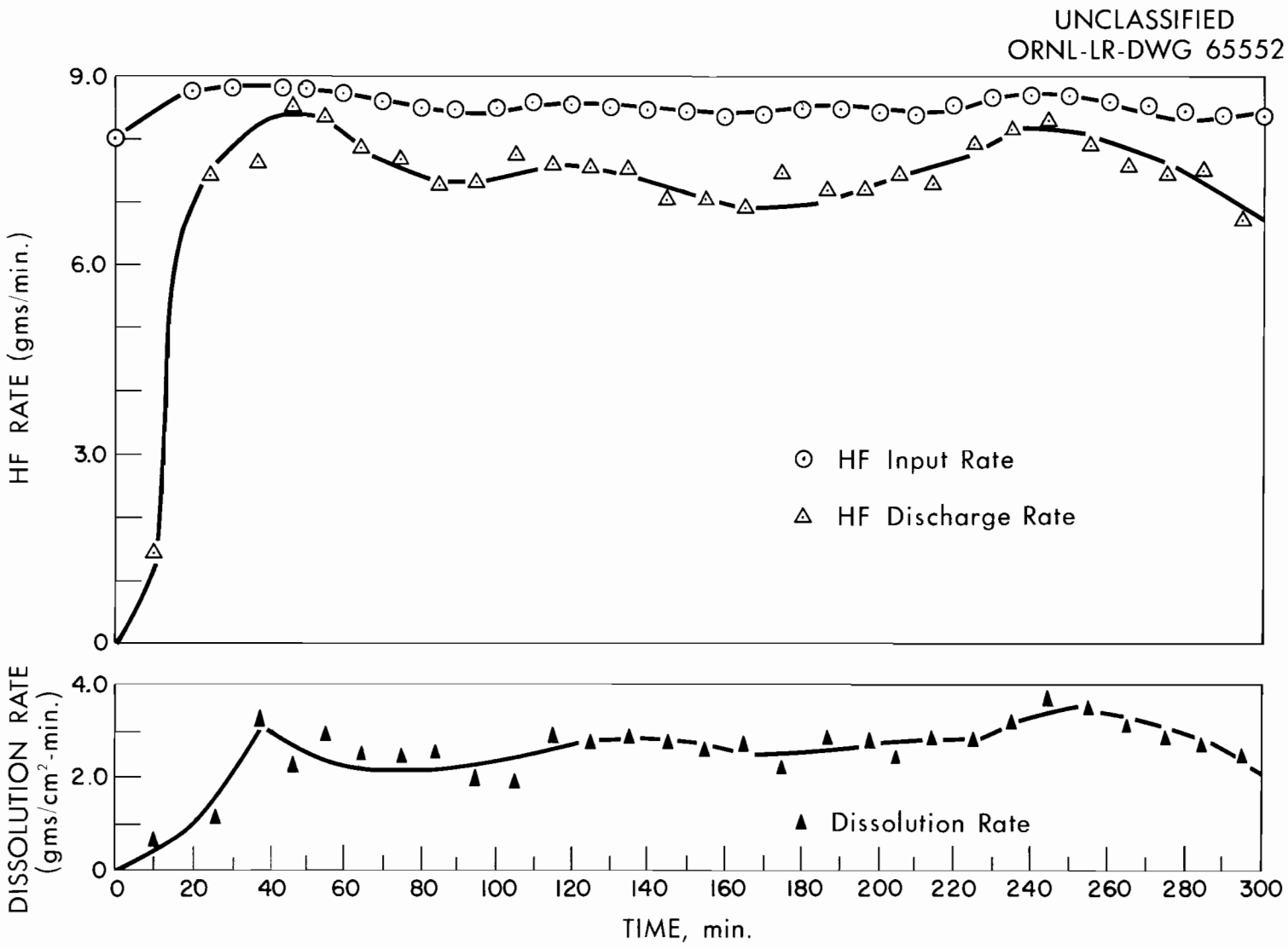

Fig. 5.3. Zirconium metal dissolution run DO-5.

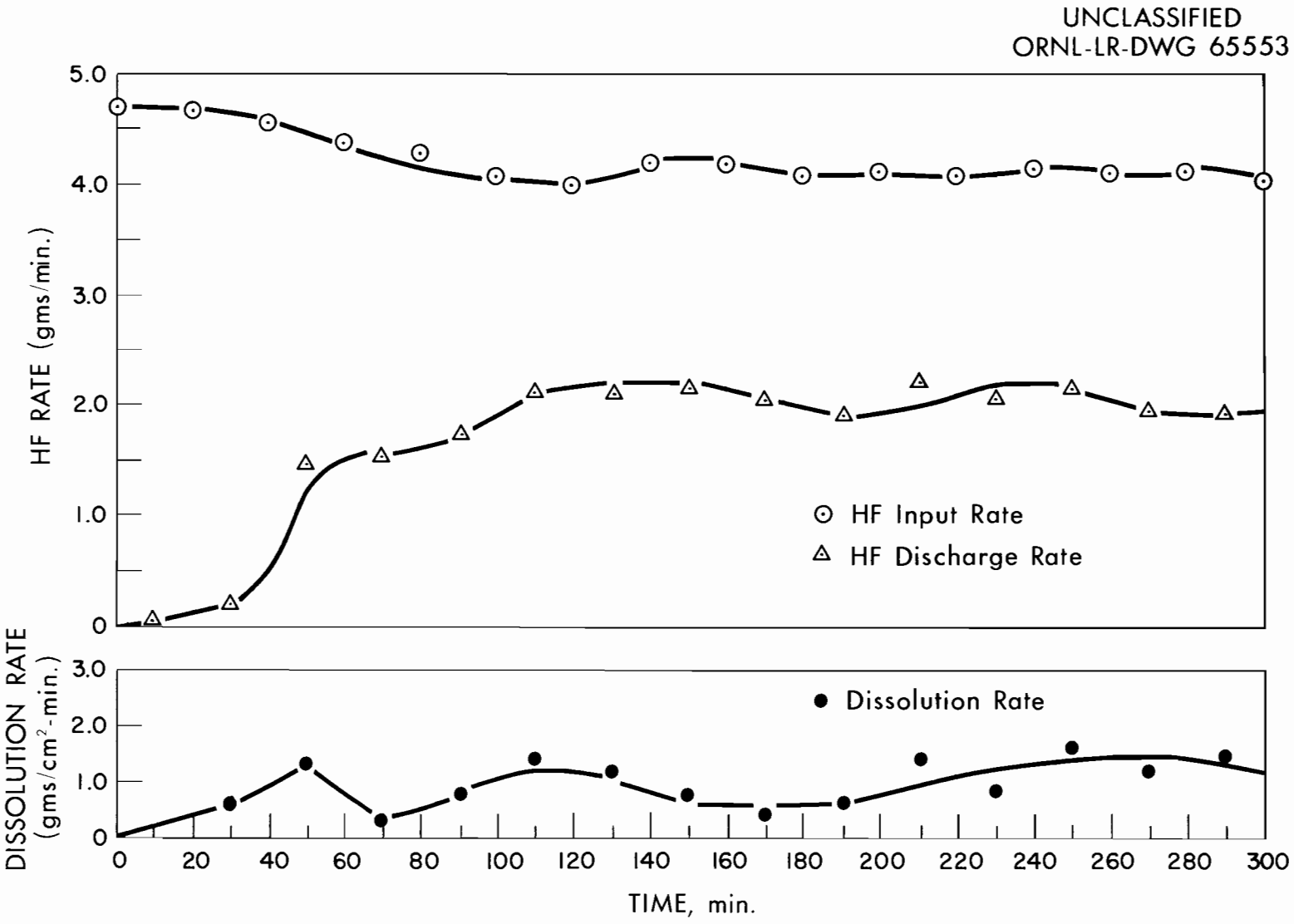

Fig. 5.4. Zirconium metal dissolution run DO-6.

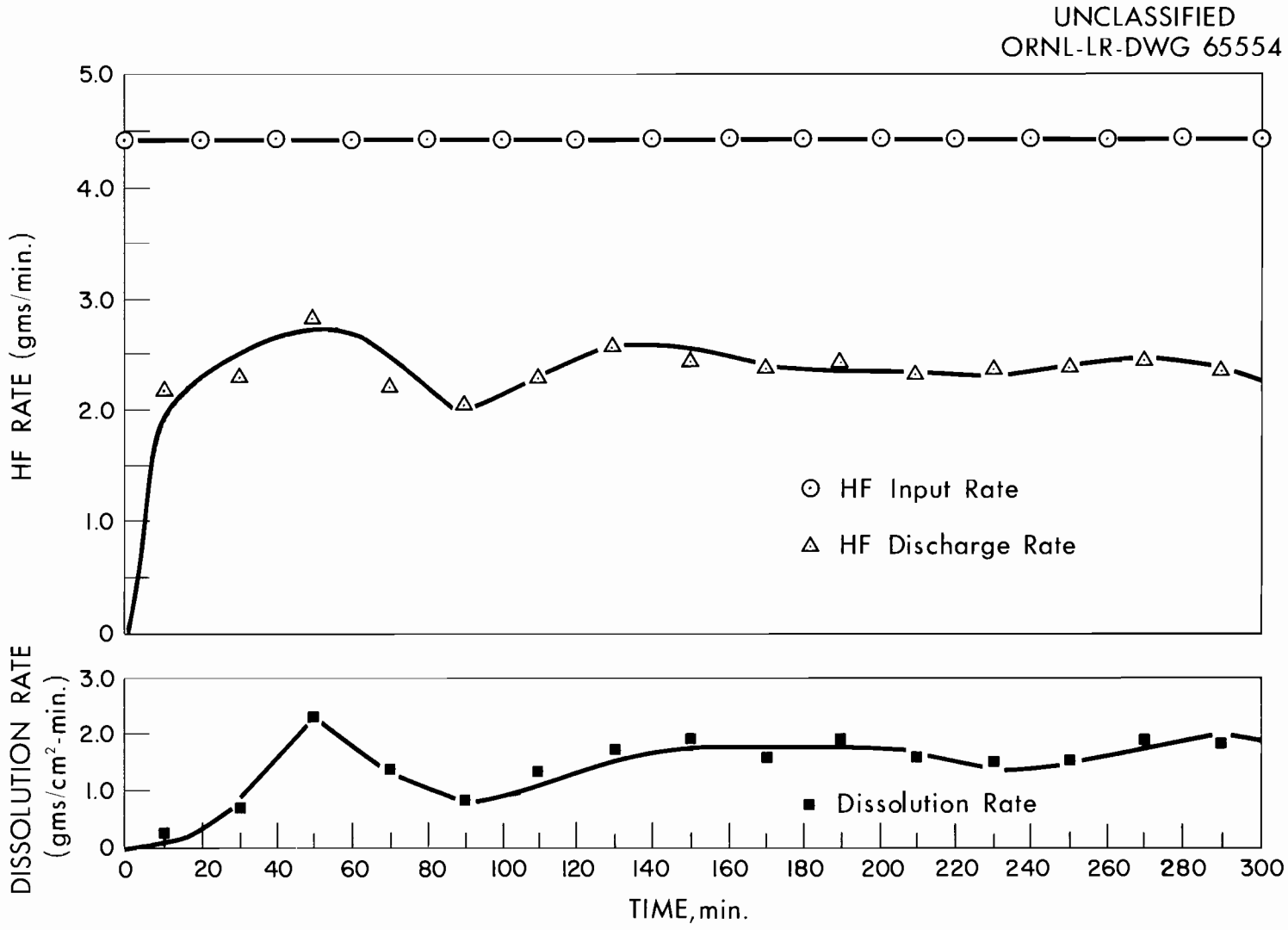

Fig. 5.5. Zirconium metal dissolution run DO-7.

Table 5.1. Averaged Dissolution Rates

Run No.	Material being Dissolved	Dissolution Rate, mg/cm^2-min By H_2O or H_2 evolved	Dissolution Rate, mg/cm^2-min By Element Wt Loss	Average HF Rate g/min
DO-4	Zr	1.5	1.3	8.5
DO-5	ZrO_2	2.5	1.9	8.5
DO-6	ZrO_2	1.0	1.9	4.2
DO-7	ZrO_2	1.4	1.8	4.5
DO-8	Zr	0.6	0.4	1.9

DISTRIBUTION

1. E. L. Anderson (AEC Washington)
2. F. P. Baranowski (AEC Washington)
3. W. G. Belter (AEC Washington)
4. S. Bernstein (Paducah)
5. R. E. Blanco
6. J. O. Blomeke
7-10. J. C. Bresee
11. R. E. Brooksbank
12. K. B. Brown
13. F. R. Bruce
14. J. A. Buckham (ICPP)
15. L. P. Bupp (HAPO)
16. W. D. Burch
17. W. H. Carr
18. G. I. Cathers
19. J. T. Christy (HOO)
20. W. E. Clark
21. V. R. Cooper (HAPO)
22. K. E. Cowser
23. F. E. Croxton (Goodyear Atomic)
24. F. L. Culler, Jr.
25. W. Davis, Jr.
26. O. C. Dean
27. D. E. Ferguson
28. L. M. Ferris
29. R. J. Flanary
30. E. R. Gilliland (MIT)
31. H. E. Goeller
32. M. J. Googin (Y-12)
33. H. B. Graham
34. A. T. Gresky
35. P. A. Haas
36. M. J. Harmon (HAPO)
37. F. E. Harrington
38. L. P. Hatch (BNL)
39. O. F. Hill (HAPO)
40. J. M. Holmes
41. R. W. Horton
42. A. R. Irvine
43. G. Jasny (Y-12)
44. H. F. Johnson
45. W. H. Jordan
46. S. H. Jury
47. K. K. Kennedy (IDO)
48. B. B. Klima
49. E. Lamb
50. D. M. Lang
51. S. Lawroski (ANL)
52. R. E. Leuze
53. W. H. Lewis
54. J. A. Lieberman (AEC Washington)
55. R. B. Lindauer
56. A. P. Litman
57. J. T. Long
58. B. Manowitz (BNL)
59. J. L. Matherne
60. J. A. McBride (ICPP)
61. J. P. McBride
62. W. T. McDuffee
63. R. A. McGuire (ICPP)
64. R. P. Milford
65. J. W. Morris (SRP)
66. E. L. Nicholson
67. J. R. Parrott
68. F. S. Patton, Jr. (Y-12)
69. H. Pearlman (AI)
70. R. H. Rainey
71. J. T. Roberts
72. K. L. Rohde (ICPP)
73. C. A. Rohrmann (HAPO)
74. A. D. Ryon
75. W. F. Schaffer, Jr.
76-78. E. M. Shank
79. M. J. Skinner
80. C. M. Slansky (ICPP)
81. S. H. Smiley (ORGDP)
82. J. I. Stevens (ICPP)
83. C. E. Stevenson (ANL, Idaho)
84. K. G. Steyer (General Atomics)
85. E. G. Struxness
86. J. C. Suddath
87. J. A. Swartout
88. F. M. Tench (Y-12)
89. V. R. Thayer (duPont, Wilmington)
90. W. E. Unger
91. J Vanderryn (AEC ORO)
92. F. M. Warzel (ICPP)
93. C. D. Watson
94-123. M. E. Whatley
124. G. C. Williams
125. R. H. Winget
126. R. G. Wymer
127-128. Central Research Library
129-132. Laboratory Records
133. Laboratory Records (RC)
134. Document Reference Section
135. Research and Development Division
136-150. DTIE